ELSEVIER

Coordination Chemistry Reviews
165 (1997) 239–266

COORDINATION CHEMISTRY REVIEWS

Application of transient vibrational spectroscopies to the excited states of metal polypyridyl complexes

Jon R. Schoonover [a,*], Carlo A. Bignozzi [b], Thomas J. Meyer [c]

[a] *Mail Stop J586, Bioscience and Biotechnology Group (CST-4), Los Alamos National Laboratory, Los Alamos, NM 87545, USA*
[b] *Dipartimento di Chimica, Univ. di Ferrara, Ferrara, Italy*
[c] *Chemistry Department, Venable and Kenan Laboratories, The University of North Carolina at Chapel Hill, Chapel Hill, NC 27599-3290, USA*

Received 20 August 1996; received in revised form 6 March 1997

Contents

Abstract

Time-resolved resonance Raman and infrared spectroscopies have been applied to a variety of problems arising in excited states and molecular assemblies based on polypyridyl complexes of Re(I), Ru(II) and Os(II). Application of transient resonance Raman spectroscopy has

* *Corresponding author.*

PII S0010-8545(97)00016-7

been used to assign the acceptor ligand in heteroleptic Ru(II) complexes and to characterize molecular structure in acceptor ligands. It has been applied to intramolecular electron transfer in chromophore-quencher complexes and molecular assemblies and to intramolecular energy transfer in polynuclear complexes. Time-resolved infrared spectroscopy has opened new avenues for the study of excited-state electronic structure and dynamics by the observation of ν(CO) and ν(CN) bands in transient absorption difference spectra. This technique has been applied to distinguishing between metal-to-ligand charge transfer and ligand-based $\pi\pi^*$ states in Re(I) complexes and to intramolecular energy transfer in cyano-bridged oligomers. © 1997 Elsevier Science S.A.

1. Introduction

Polypyridyl complexes of d^6 transition metals have played and continue to play an important role in the study of photoinduced electron and energy transfer [1]. Molecular assemblies based on these complexes are being studied for applications in artificial photosynthesis and the fabrication of molecular-level devices. They are being used as molecular sensors and, when attached to metal oxide surfaces, as sensitizers for photon-to-electrical energy conversion. Their excited states have provided fundamental information on the effects of structural change in the acceptor ligand, the energy gap and the medium on nonradiative decay. The dynamic spectroscopies used to probe these phenomena have been based largely on emission and absorption measurements but the underlying spectral bands are characteristically broad and featureless because of coupling with intramolecular vibrations and the solvent. They seldom provide direct insight into the electronic character of the state, or states, that are reached and provide a limited amount of information about molecular structure. Additional insight is required to gain an in-depth understanding of the electronic and molecular structures of excited states or intermediates and how they relate to photochemical and photophysical properties.

Vibrational spectroscopies (infrared and Raman) can help to overcome this problem by their "fingerprinting" possibilities and the information they give about molecular structure. They are structure-specific and can provide much information about excited states and intermediates [2]. With the advent of fast and ultrafast laser systems, time-resolved infrared and Raman data can now be acquired on time scales ranging from microseconds to femtoseconds [3]. These techniques have been successfully applied to a variety of excited-state phenomena based on polypyridyl complexes and their molecular assemblies. This account provides a summary.

2. Time-resolved resonance Raman

2.1. Theory

The ability to measure short-lived, transient Raman spectra of photophysical and photochemical intermediates is due to advances in laser and detector technology

and the existence of the resonance Raman effect. Resonance enhancements of Raman scattering occur when the wavelength of the incident light is near or within an electronic absorption band of the sample. This can increase the intensity of the scattered light by four to six orders of magnitude making this an extremely sensitive and selective probe for transients even in dilute solutions.

The intensity of Raman scattering is given by Eq. (1). In this equation the Raman tensor, $\boldsymbol{R}_{\rho\sigma}$, is defined in Eq. (2).

$$I(\nu_r)=(\text{constant})(\nu_r)^4 I(\nu_0)\sum_{\rho\sigma}|\boldsymbol{R}_{\rho\sigma}|^2 \tag{1}$$

$$\boldsymbol{R}_{\rho\sigma}=(\alpha_{\rho\sigma})\boldsymbol{E} \tag{2}$$

ν_0 is the frequency of the incident light, ν_r is the Raman frequency and ρ, σ are the x, y or z components of $\boldsymbol{R}_{\rho\sigma}$. $\alpha_{\rho\sigma}$ is the ρ^{th} and σ^{th} element of the polarizability tensor and $\boldsymbol{E}$ is the electric vector of the incident light. A quantum mechanical treatment of the Raman polarizability tensor provides an expression for the intensity of Raman scattering which accounts for resonance enhancement. Second order perturbation theory for the polarizability, induced by electromagnetic radiation gives

$$(\alpha_{\rho\sigma})_{gf}=\sum_e\left[\frac{\langle f|\mu_\rho|e\rangle\langle e|\mu_\sigma|g\rangle}{(\nu_{ge}-\nu_0+i\Gamma_e)}\right]+\left[\frac{\langle f|\mu_\sigma|g\rangle\langle e|\mu_\rho|g\rangle}{(\nu_{ge}\times\nu_0+i\Gamma_e)}\right] \tag{3}$$

The $|g\rangle$ and $|f\rangle$ are the initial and final state wavefunctions (electronic and nuclear). μ_ρ and μ_σ are dipole moment operators. $|e\rangle$ is the wavefunction of an excited state. ν_{ge} and ν_{ef} are the transition frequencies from g to e and from e to f. ν_0 is the frequency of the laser line and $i\Gamma_e$ is a damping factor [4]. In resonance Raman scattering, ν_0 approaches ν_{ge}. The first term in Eq. (3) dominates and is responsible for the resonance effect. Application of the Born–Oppenheimer approximation allows the wavefunctions to be separated into electronic and vibrational parts. Albrecht has derived a more detailed equation by expansion of the electronic wavefunctions [5].

A calculationally and conceptionally useful alternate theoretical description of the resonance Raman effect has been derived by Heller [6]. The Heller theory utilizes the time domain and exploits the fact that Raman scattering is a short-timescale process, occurring in a small fraction of the period of a molecular vibration. There is, therefore, no need to know the vibrational eigenstates of the excited electronic state because there is insufficient time for them to be resolved. The advantage of this approach is the use of wave packet dynamics which allow Raman intensities to be viewed as the result of a classical force exerted by the excited-state potential surface at the equilibrium nuclear coordinate of the ground state. This approach stresses the temporal evolution of the scattering process and results in a more realistic and practical guide for the interpretation of resonance Raman intensities. Expressions are derived relating relative Raman intensities to the frequency (or angular frequency $\omega_j=2\pi\nu_j$) and dimensional displacement, Δ_j, on a mode-by-mode basis for all coupled vibrations, j. In one limit of approximation the relative intensities

of two resonantly enhanced Raman bands are given by

$$\frac{I_1}{I_2} = \frac{(\omega_1^3 A_1^2)}{(\omega_2^3 A_2^2)} \tag{4}$$

This gives insight into excited-state structure since the individual A_j's are related to the change in equilibrium displacement between excited and ground state, $\Delta Q_{e,j}$, by

$$A_j = \left(\frac{2\mu_j \omega_j}{\hbar}\right)^{\frac{1}{2}} (\Delta Q_{e,j}) = \left(\frac{2f_j}{\hbar\omega_j}\right)^{\frac{1}{2}} (\Delta Q_{e,j}) \tag{5}$$

μ_j and f_j are the reduced mass and force constant for the normal mode in the ground state. The changes in local bond displacements and difference in structure between excited and ground states are given by the sum of the $\Delta Q_{e,j}$ for the individual normal modes.

The first time-resolved resonance Raman study on a transition metal complex was reported by Dallinger and Woodruff on $[Ru(bpy)_3]^{2+*}$ (bpy is 2,2′-bipyridine) [7].

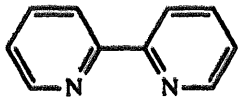

The data showed that the metal-to-ligand charge transfer (MLCT) excited state reached following laser flash photolysis could be described as $[Ru^{III}(bpy)_2(bpy^{\cdot -})]^{2+*}$ rather than as the delocalized form $[Ru^{III}(bpy^{\cdot -1/3})_3]^{2+*}$. In subsequent studies the question of localization in mixed-chelate polypyridyl Ru(II) complexes was investigated in further detail [8]. These results (through 1986) were reviewed by Morris and Woodruff [2]a. More recent studies have included normal coordinate analyses of the ground and MLCT excited states of $[Ru(bpy)_3]^{2+}$ and application of ultrafast techniques [2]e–g,n.

2.2. *Instrumentation*

In Fig. 1 is shown a schematic diagram of one approach to nanosecond time-resolved resonance Raman spectroscopy. When coupled with a spectrograph, the use of multichannel detection systems such as a charge-coupled device (CCD) allows a complete spectrum to be measured with a single laser pulse. Spectra can be "time-resolved" by operating the detector in a gated mode. The single laser pulse is used to both excite the sample and as a source for the Raman scattering. The intensity of the pulse must be sufficient to promote a large majority of molecules into the excited state. Therefore, the first part of the pulse (within the focus of the laser pulse) excites the sample and the remaining part is used as the source for the Raman scattering. The Raman signal is integrated over the gate period which is centred over the laser pulse. Given this arrangement, a precise definition of time resolution is not straightforward. However, in practical terms the excited states accessible by this approach must have lifetimes of 20 ns or longer and the resulting spectrum can

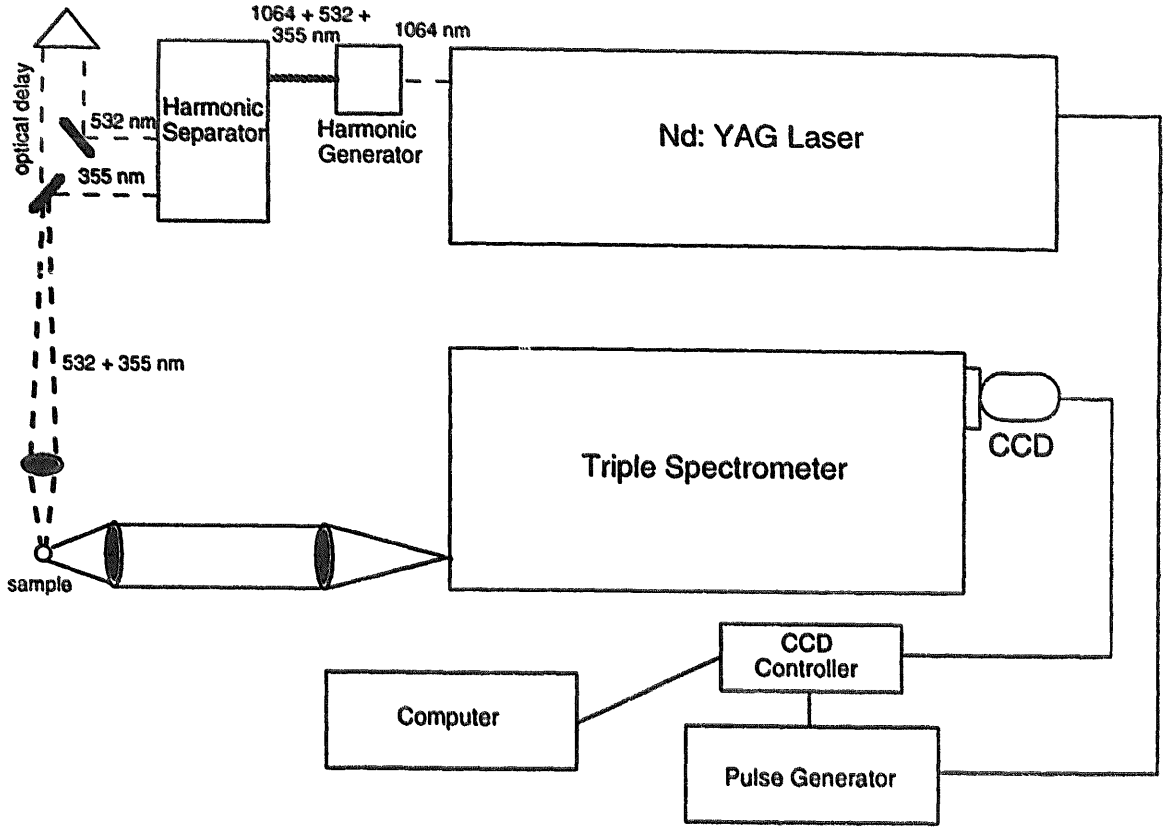

Fig. 1. Nanosecond time-resolved resonance Raman apparatus. The experiment can be conducted in one of two ways: (1) The third harmonic of a Nd:YAG laser (354.7 nm) can be used to both excite the sample and as a source for the Raman scattering. Time resolution is provided by a gated detector. (2) The second harmonic (532 nm) can be used as a pump pulse to excite the sample, while the optically delayed 354.7 nm pulse can be used as the probe pulse. Time resolution is provided by the timing between the pump and probe pulse.

be considered as an average of the true excited-state resonance Raman spectra over the integration time.

Time resolution can be improved by using two color pump–probe experiments. In this configuration one laser pulse is used to create the excited state or photochemical intermediate and the second is the source for Raman scattering. Time resolution is achieved by control of the time delay between the pump and probe pulses. With picosecond laser systems the time resolution can be extended to a few picoseconds.

2.3. Applications

2.3.1. Heteroleptic complexes

The most straightforward use of time-resolved resonance Raman spectroscopy is identification of excited states or intermediates by fingerprinting. A great deal of molecularly specific information is available in infrared and Raman spectra. Even slight changes in structure lead to discernible changes in spectra. For example, changes in the peripheral substituents on bpy from H's in the 4 and 4′ positions to

methyl groups is sufficient to produce discernibly different MLCT-enhanced resonance Raman spectra. This provides a definitive basis for establishing the acceptor ligand in mixed-ligand complexes [2,8]. This is illustrated by the transient Raman spectra for $[Ru(bpy)_3]^{2+*}$, $[Ru(dmb)_3]^{2+*}$, $[Ru(bpm)_3]^{2+*}$ and $[Ru(bpy)(dmb)(bpm)]^{2+*}$ (dmb is 4,4′-$(Me)_2$bpy; bpm is 2,2′-bipyrimidine, see below) in Fig. 2 [9]. In $[Ru(bpy)(dmb)(bpm)]^{2+*}$ resonance Raman bands for $bpm^{\cdot -}$ dominate the transient spectrum following 354.7 nm excitation. This is a region of intense $\pi \rightarrow \pi^*$ absorption for the various ligand radical anions. There is no evidence for enhancement from $bpy^{\cdot -}$ or $dmb^{\cdot -}$-based bands. This leads to formulation of the excited state as $[Ru(bpy)(dmb)(bpm^{\cdot -})]^{2+*}$ which is consistent with electrochemical measurements showing that bpm is the lowest-lying π^* acceptor ligand.

In terms of the fingerprinting aspect of the Raman approach, the spectral shifts between bpy and dmb as the acceptor ligand in Fig. 2 are slight, but characteristic. The bands from 1000–1700 cm^{-1} have their origins in normal modes largely C–C and C–N stretching in character but mixed with some C–H bending [2]n.

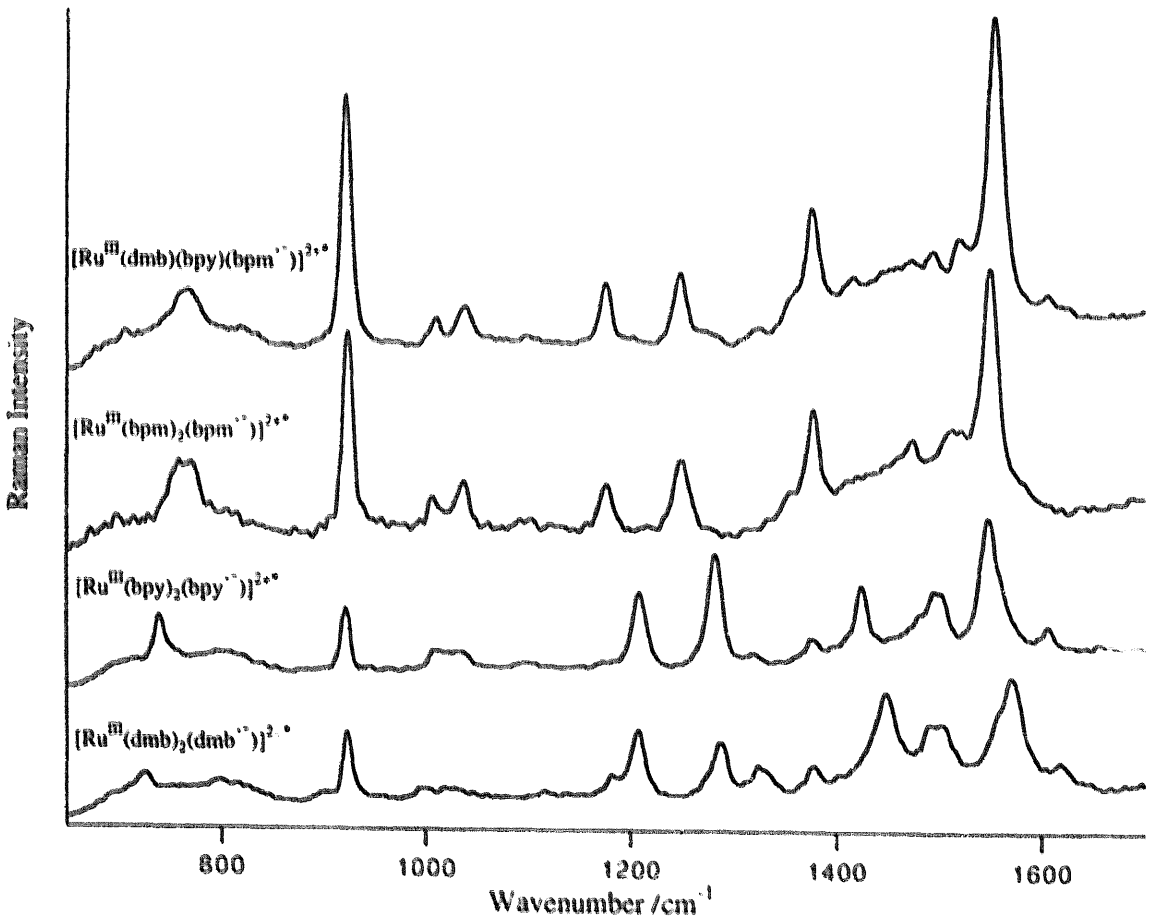

Fig. 2. Transient resonance Raman spectra from 700 to 1700 cm^{-1} for $[Ru(bpy)_3]^{2+*}$, $[Ru(dmb)_3]^{2+*}$, $[Ru(bpm)_3]^{2+*}$ and $[Ru(bpy)(dmb)(bpm)]^{2+*}$ (bpy is 2,2′-bipyridine; dmb is 4,4′-$(Me)_2$bpy; bpm is 2,2′-bipyrimidine) measured in CH_3CN at room temperature. The spectra were acquired by using 354.7 nm laser pulses to excite the sample and as a source for the Raman scattering. A complete description of the experimental apparatus and data acquisition conditions can be found in Ref. [24]b.

2.3.2. Characterization of acceptor ligands

Transient resonance Raman measurements have been instructive in establishing structural details and the role they play in excited state decay for the acceptor ligands *trans*-1,2-bis(4-(4′-methyl)-2,2′-bipyridyl)ethane (bbpe) and dipyrido[3,2-*a*:2′,3′-*c*]phenazine (dppz).

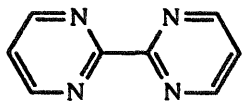

bpm

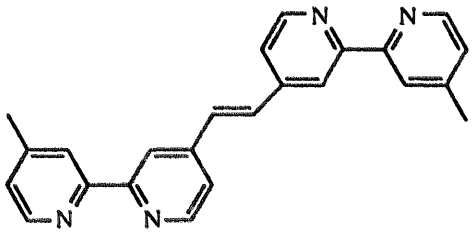

bbpe

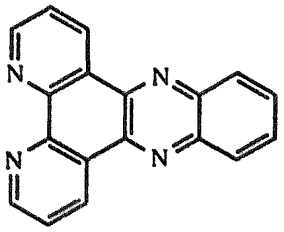

dppz

Relative to comparable MLCT emitters, the MLCT excited state of $[(dmb)_2Ru(\mu\text{-bbpe})Ru(dmb)_2]^{4+}$ is unusually long-lived, $\tau = 1310$ ns in CH_3CN at 298 K for its emission maximum at 750 nm, (13 000 cm^{-1}). For comparison $[Ru(dmb)_3]^{2+*}$ emits at 624 nm (15 600 cm^{-1}) and has $\tau = 950$ ns. [10] This is a surprise since MLCT lifetimes typically decrease with emission energy.

The origins of this effect are well understood. MLCT excited-state decay is typically dominated by nonradiative decay and k_{nr} varies with the energy gap, E_0, as in Eq. (6). This is a form of the famous energy gap law. It uses mode averaging with the quantum spacing for an averaged acceptor mode ($\hbar\omega$) and the associated electron-vibrational coupling constant (S). S is related to Δ by, $S = 0.5(\Delta^2)$. It is a measure of the change in equilibrium displacement between states – the degree of excited-state distortion.

$$k_{nr} \propto \exp\left(\frac{-\gamma E_0}{\hbar\omega}\right) \tag{6}$$

$$\gamma = \ln\left(\frac{E_0}{S\hbar\omega}\right) - 1 \tag{7}$$

Eq. (6) correctly predicts that k_{nr} decreases with E_0. This is a general prediction independent of the acceptor ligand. The acceptor ligand appears in γ in the magnitude of S and the degree of excited state distortion to E_0. The difference between dmb and bbpe as acceptor ligands is that S is smaller for bbpe.

This is seen in resonance Raman intensity comparisons, which show that the intensities of polypyridyl ring stretching bands are significantly decreased relative

to $[Ru(dmb)_3]^{2+}$. From Eq. (4), relative intensities vary with Δ_j^2 (and $\Delta Q_{e,j}^2$). The same conclusion is reached by fitting emission spectra with a Franck–Condon analysis and a single averaged acceptor mode. This also shows that S is smaller for bbpe.

The microscopic origin of this effect is well understood. Delocalization of the excited electron over the expanded molecular framework of bbpe compared to bpy and dmb results in diminished electron–electron repulsion and smaller changes in local bond displacements between ground and excited states. As illustrated in Fig. 3, this diminishes ΔQ_e and S, and with them the degree of vibrational wavefunction overlap. k_{nr} depends on the square of the vibrational overlap integral because it defines the extent to which the two states are coincident along the normal coordinate.

In fact, for these polypyridyl complexes a series of ring-stretching vibrations from 1000–1600 cm^{-1} typically dominate as energy acceptors. The electron-vibrational coupling constant is the sum of the S_j for the coupled vibrations (those with $\Delta Q_{eq,j} \neq 0$),

$$S = \sum_j S_j \tag{8}$$

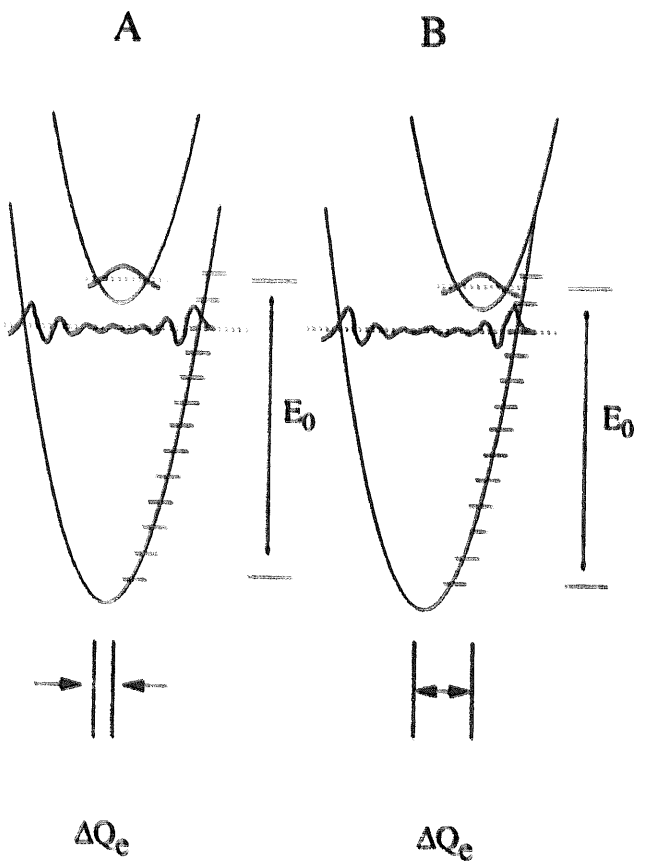

Fig. 3. The effect of variations in ΔQ_e on vibrational wavefunction overlap for the case with $\Delta Q_e(B) > \Delta Q_e(A)$.

and $\hbar\omega$ the weighted sum of the $\hbar\omega_j$'s

$$\hbar\omega = \frac{\sum_j (S_j \hbar\omega_j)}{(\sum_j S_j)} \tag{9}$$

In $[(dmb)_2Ru(\mu\text{-}bbpe)Ru(dmb)_2]^{4+}$ fingerprinting comparisons of resonance Raman spectra clearly point to bbpe as the acceptor ligand in the excited state. The –C=C– stretch of the olefin bridge shifts from 1638 cm^{-1} in the ground state to 1578 cm^{-1} in the excited state. The C(ring)–C(olefin) stretch shifts from 1186 to 1255 cm^{-1}. Both are consistent with delocalization of the excited electron across the olefin link. Similar changes have been found in comparing Raman data for *trans*-stilbene and bbpe with their radical anions [11].

It was originally suggested that following MLCT excitation of $[Ru(bpy)_2(dppz)]^{2+}$ (dppz is dipyrido[3,2-*a*:2′,3′-*c*]phenazine) with dppz as the acceptor that the excited electron was localized on the phenazine portion of the ligand [12]. An alternate description is that the excited electron occupies a delocalized molecular orbital. Electron density may be concentrated on the phenazine, but there is significant bpy (or phen) character as well.

Comparison of ground- and excited-state resonance Raman spectra between $[Ru(bpy)_2(dppz)]^{2+}$ and $[Ru(dmb)_2(dppz)]^{2+}$ (CH_3CN, 298 K) clearly reveal that dppz is the acceptor. Resonantly enhanced Raman bands for $bpy^{\cdot -}$ or $dmb^{\cdot -}$ are not observed in the excited states. The bands that do appear are very similar to those for $dppz^{\cdot -}$ generated electrochemically.

The excited state spectra can be simulated as a combination of the $phen^{\cdot -}$ Raman bands that appear in the transient spectrum of $[Ru(phen)_3]^{2+*}$ (phen is 1,10-phenanthroline) and $phenazine^{\cdot -}$ from the spectrum of the electrochemically generated anion [13]. This points to coupled vibrations at both the phenazine and phen portions of the ligand consistent with delocalization of the excited electron over the phen portion of the ligand as well.

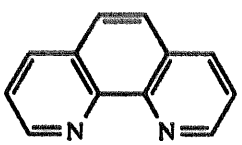

phen

The excited state dppz bands are only slightly shifted compared to the ground state bands. The ring vibration near 1400 cm^{-1} that dominates the ground-state resonance Raman spectrum of phenazine shifts by only -4 cm^{-1} in $[Ru(dmb)_2(dppz)]^{2+*}$. It shifts -56 cm^{-1} in electrochemically generated $phenazine^{\cdot -}$. Phen-localized bands at 1576 and 1597 cm^{-1} shift -29 and -19 cm^{-1} in the excited state compared to -45 and -29 cm^{-1} in $[Ru(phen)_3]^{2+*}$. These results are also consistent with phen character in the dppz acceptor level and delocalization of the excited electron over the entire ligand framework.

In a related study, Kincaid's group has applied transient resonance Raman to the

question of electronic structure in inherently asymmetrical acceptor ligands [14]. They studied Ru^{II} complexes containing 2-(2-pyridyl)pyrazine (pypz), 4-methyl-2,2′-bipyridine or 5-methyl-2,2′-bipyridine. In the ground-state resonance Raman spectra of $[Ru(bpy)_2(pypz)]^{2+}$ and various deuterated versions, a set of bands appear which can be assigned to the pyridine portion of the ligand. Another set can be assigned to the pyrazine portion. Bands due to inter-ring modes and modes arising from the stretching of adjacent bonds in the different rings are also enhanced. Based on the shifts in band energies between excited and ground states, it was suggested that electron density is highly polarized toward the pyrazine portion of the ligand in the lowest excited state.

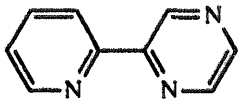

pypz

2.3.3. Intramolecular electron transfer

Transient absorption and emission have been the methods of choice for studying light-induced electron transfer in chromophore-quencher complexes and molecular assemblies [15]. Transient resonance Raman offers a complementary technique which can be very helpful in identifying intermediates and establishing structural details [16]. Mode-specific information is available and changes in structure and conformation induced by electron transfer can often be inferred from changes in band energies and relative intensities.

Time-resolved resonance Raman spectroscopy has been applied to the structural changes that occur in *N*-methyl-4,4′-bipyridinium cation (monoquat or MQ^+) when it acts as the acceptor ligand. Based on transient absorption measurements on *fac*-$[(bpy)Re(CO)_3(MQ^+)]^{2+}$ $d\pi(Re^I) \rightarrow \pi^*(bpy)$ excitation is followed by $bpy^- \rightarrow MQ^+$ electron transfer which occurs to give the lower energy, $Re^{II}(MQ^-)$-based MLCT excited state in Scheme 1 [14]a. The same state is reached directly by simultaneous $Re^I \rightarrow MQ^+$ excitation. Electrochemical measurements show that MQ^+ is a better acceptor than bpy by ~0.5 V.

Transient resonance Raman spectra (600–1700 cm^{-1}) of the excited states of *fac*-$[Re(bpy)(CO)_3(4\text{-Etpy})]^+$ (4-Etpy is 4-ethylpyridine) and *fac*-$[Re(bpy)(CO)_3(MQ^+)]^{2+}$ (CH_3CN, 298 K, 354.7 excitation, 354.7 nm probe) are shown in Fig. 4. For the MQ^+ complex the same bands are resonantly enhanced as in *fac*-$[Re^I(bpy)(CO)_3(MQ^-)]^+$ generated by electrochemical reduction. Bpy^--based bands are not enhanced showing that $bpy^- \rightarrow -MQ^+$ electron transfer is complete in the 100 ns timescale of the experiment. The spectrum of *fac*-$[Re(bpy)(CO)_3(4\text{-Etpy})]^{+*}$ is typical of bpy as an acceptor [7,17].

Vibrational analyses have been conducted on molecules that are structurally related to MQ^+ and their one-electron reduced forms. These include biphenyl and *N*,*N*′-dimethyl-4,4′-bipyridinium dication (paraquat or PQ^{2+}) [18,19]. Comparison

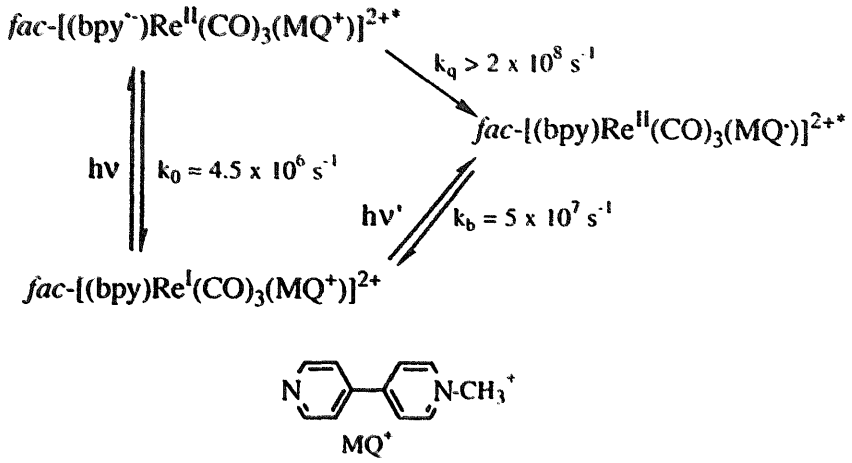

Scheme 1. (in CH_3CN at 298 K).

with the excited-state data reveal that significant structural changes occur at $-MQ^+$ when it accepts an electron. An inter-ring C–C stretch at $\sim 1300\,cm^{-1}$ in the ground state shifts to $1360\,cm^{-1}$ in the excited state. There are similar shifts in the one-electron reduced forms of biphenyl, 4,4′-bpy (4,4′-bpy is 4,4′-bipyridine) and PQ^{2+}. In *fac*-$[Re^I(bpy)(CO)_3(MQ^{\bullet})]^+$ generated electrochemically, the shift is $+50\,cm^{-1}$. In *fac*-$[Re^{II}(bpy)(CO)_3(MQ^{\bullet})]^{2+}$ it is $+61\,cm^{-1}$. The shifts to higher

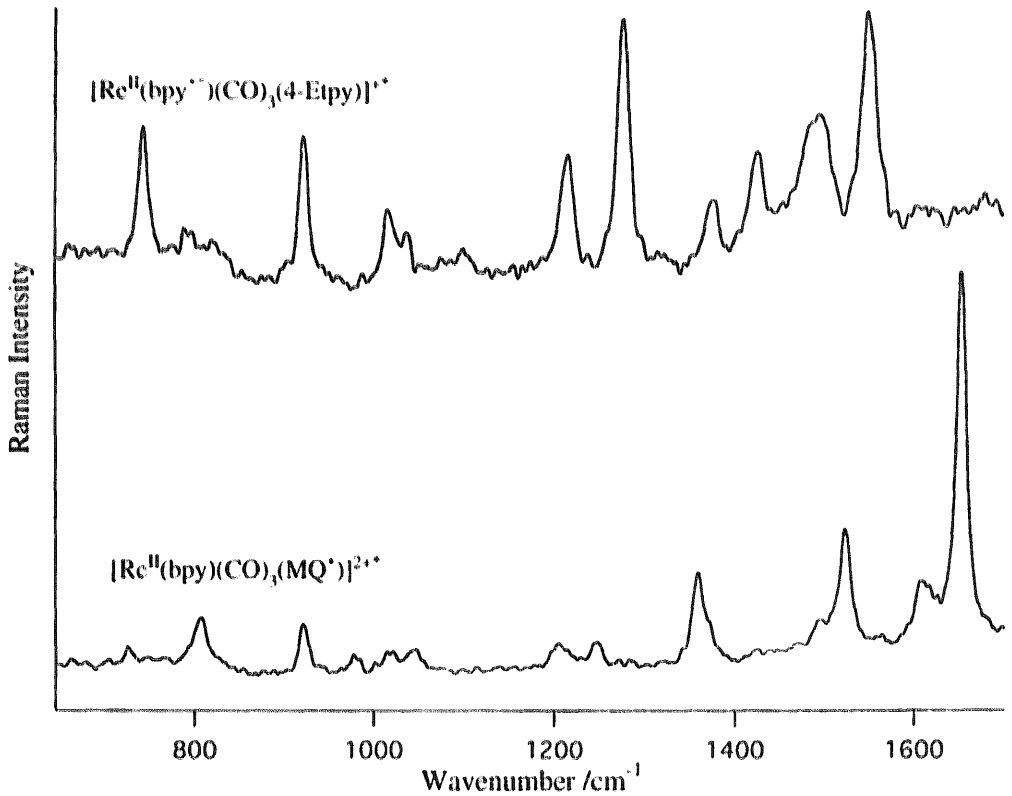

Fig. 4. Transient resonance Raman spectra ($700–1700\,cm^{-1}$) of *fac*-$[Re(bpy)(CO)_3(4\text{-}Etpy)]^{+*}$ and *fac*-$[Re(bpy)(CO)_3(MQ^+)]^{2+*}$, as in Fig. 1.

energy are consistent with an increase in –C–C– bond order and a decrease in the inter-ring separation distance. These structural changes are consistent with a planar, quinoidal structure in the excited state with the angle (θ) between pyridyl planes near 0°.

The ground- and excited-state Raman data combine to provide a relatively clear picture of the structural changes that accompany electron transfer to $-MQ^+$. From X-ray crystallography $\theta \sim 47°$ in the ground state of *fac*-[Re(bpy)$(CO)_3(MQ^+)]^{2+}$. This angle represents a balance between H···H repulsion between the linked rings, which is minimized at $\theta = 90°$, and electronic delocalization, which is maximized at $\theta = 0°$. Upon electron transfer to MQ^+, there is a change in θ from ~47° to ~0°. It is accompanied by an increase in electronic delocalization, Eq. (10). The energy difference between the $\theta \sim 47°$ and $\theta \sim 0°$ forms for *fac*-[Re(bpy)$(CO)_3(MQ^{\cdot})]^{2+*}$ is ~0.3 eV. The $\theta \sim 0°$ form is favored because of the increase in delocalization energy [20].

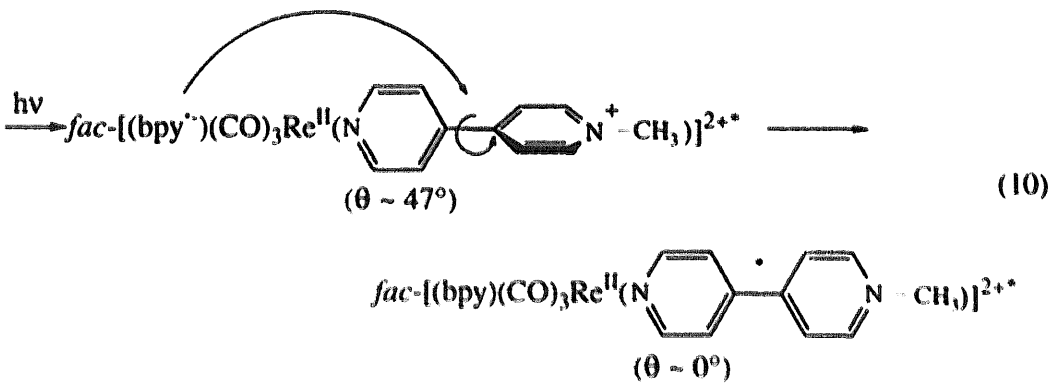

(10)

The advantage of being able to tune the laser probe beam is illustrated by a second example [17]. Following $d\pi(Re^I) \rightarrow \pi^*(bpy)$ excitation of *fac*-[Re(bpy)$(CO)_3$(py–PTZ)]$^+$ (py–PTZ is 10-(4-picolyl)phenothiazine), MLCT emission is quenched and absorption bands appear for $bpy^{\cdot -}$ (at 370 nm) and $-PTZ^{\cdot +}$ (at 510 nm). These observations are consistent with intramolecular electron transfer (Scheme 2) [15]c.

The expected bands for $bpy^{\cdot -}$ appear in transient Raman spectra acquired with 354.7 nm excitation and 354.7 nm probe pulses. Confirmation of electron transfer from $-PTZ$ is confirmed by the resonance enhancement of $-PTZ^{\cdot +}$ bands observed after 354.7 nm excitation by using 532 nm laser pulses. The $-PTZ^{\cdot +}$ spectrum obtained in the transient experiment was the same as the CW Raman spectrum ($\lambda_{ex} = 530.9$ nm) of $-PTZ^{\cdot +}$ in *fac*-[Re^I(bpy)$(CO)_3$-(py–$PTZ^{\cdot +}$)]$^{2+}$ or 10-methylphenothiazine cation [22].

The same protocol was applied to molecular assemblies based on amino acids [23]. In the transient absorption difference spectrum of [Anq–Lys(Ru^{II}(bpy)$_2$m–)–PTZ]$^{2+}$ (Anq is anthraquinone; Lys is the derivatized lysine; m is 4′-methyl-2,2′-bipyridyl-4′-carbonyl), bands appear for $-PTZ^{\cdot +}$ (510 nm) and $-Anq^{\cdot -}$ (570 nm) following $Ru^{II} \rightarrow$polypyridyl excitation consistent with Scheme 3 [24].

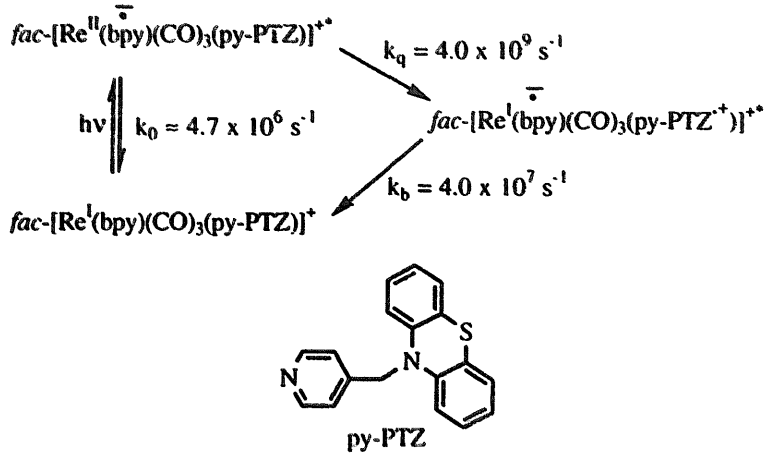

Scheme 2. (in CH_3CN at 298 K).

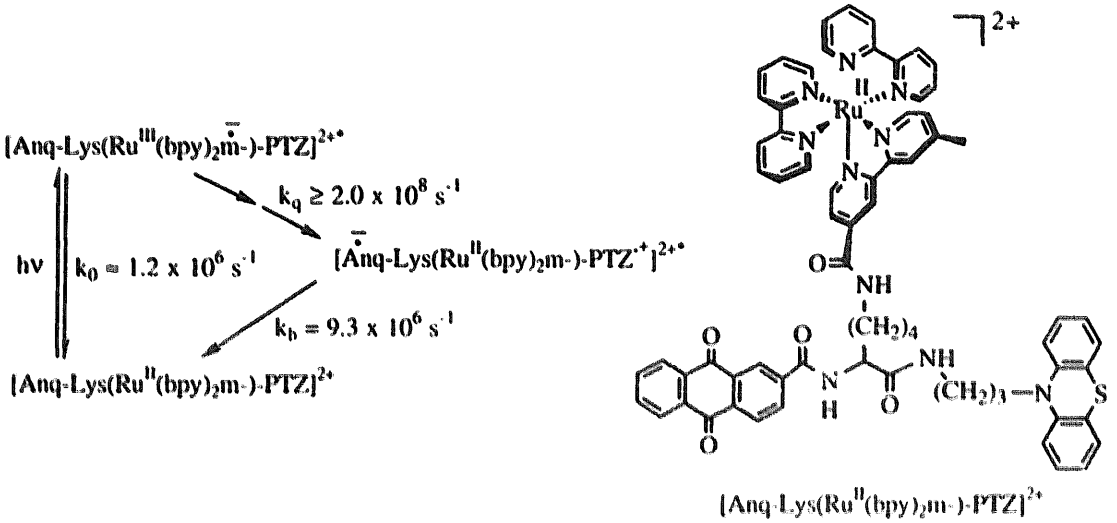

Scheme 3. (in CH_3CN at 298 K).

The transient resonance Raman spectrum (354.7 nm excitation, 354.7 nm probe) of the model $[Ru(bpy)_2(m\text{–}NHCH_3)]^{2+}$ (m is 4′-methyl-2,2′-bipyridyl-4′-methyl amide) was used to establish that the excited electron is localized on $\pi^*(m\text{–}NHCH_3)$ in the equilibrated excited state. This was made clear by fingerprinting and comparing the spectra of $[Ru(bpy)_2(m\text{–}NHCH_3)]^{2+*}$, $[Ru(bpy)_3]^{2+*}$ and $[Ru(m\text{–}NHCH_3)_3]^{2+*}$. Bands for $m\text{–}NHCH_3^{\cdot -}$ or $bpy^{\cdot -}$ were not observed in the transient spectra of the assembly consistent with rapid electron transfer following MLCT excitation. With excitation at 354.7 nm with the probe at 532 nm, resonant enhancement for the characteristic $-PTZ^{\cdot +}$ and $Anq^{\cdot -}$ bands occurred.

Raman fingerprinting has been particularly useful in establishing the quenching site or sites in assemblies where there are multiple quenchers. An example is $[(MQ^+)(CO)_3Re(\mu\text{-bbpe})Re(CO)_3(py\text{–}PTZ)]^{3+}$. Following $d\pi(Re^I) \rightarrow \pi^*(bbpe)$ excitation at 420 nm in CH_3CN, only a single, broad, nondescript absorption feature is observed from 380 to 700 nm [11]d,e. It was possible to demonstrate that both

$-MQ^{\cdot}$ and $-PTZ^{\cdot +}$ where produced by the appearance of their characteristic Raman bands following 354.7 nm excitation and either a 354.7 nm ($MQ^{\cdot}$) or 532 nm ($-PTZ^{\cdot +}$) pulse probe. Their appearance is consistent with MLCT excitation and a series of intramolecular electron transfers to give the final redox-separated state shown in Scheme 4.

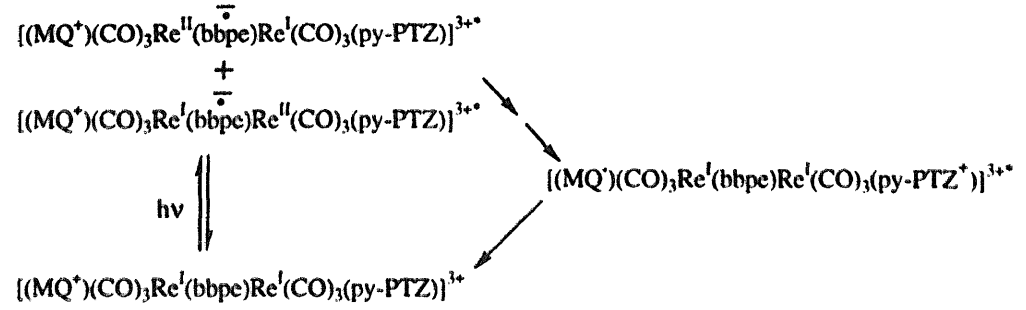

Scheme 4. (in CH_3CN at 298 K).

2.3.4. *Intramolecular energy transfer*

Transient and CW emission studies have been applied to energy transfer in cyano-bridged polynuclear complexes containing $Ru(bpy)_2^{2+}$ units. There is relatively strong electronic coupling across the cyanide bridge and intramolecular energy transfer occurs from C- to N-bonded units, Scheme 5, with unit efficiency [25]. This has led to the design of a molecular assembly for the visible sensitization of semiconductors [26], and to oligomers which act as molecular conduits for long-range energy transfer [27].

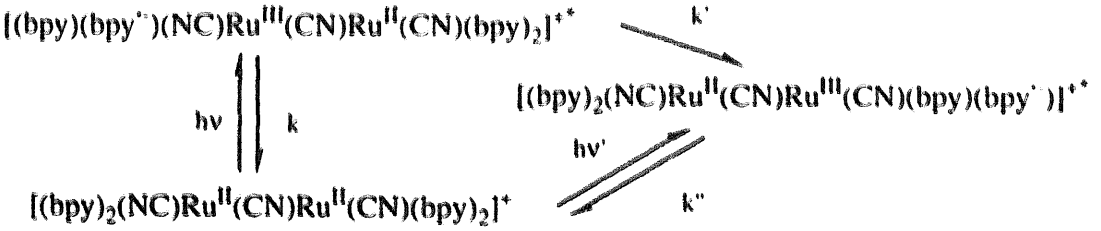

Scheme 5. (in CH_3CN at 298 K).

The existence of energy transfer was demonstrated by combining transient Raman measurements and synthesis. In the pair, $[(NC)(phen)_2Ru(CN)Ru(bpy)_2(CN)]^+$ and $[(NC)(bpy)_2Ru(CN)Ru(phen)_2(CN)]^+$, the exchange of phen for bpy is nearly equivalent electronically since the energies of the lowest-lying π^* acceptor levels for bpy and phen are nearly the same. Nonetheless, the two ligands can still be distinguished unambiguously by Raman fingerprinting of their radical anions.

In the spectrum of $[(NC)(phen)_2Ru(CN)Ru(bpy)_2(CN)]^{+*}$ in Fig. 5 only $bpy^{\cdot -}$ enhancement is observed. The phen bands that do appear are enhanced ground-state bands. In the spectrum of $[(NC)(bpy)_2Ru(CN)Ru(phen)_2(CN)]^{+*}$

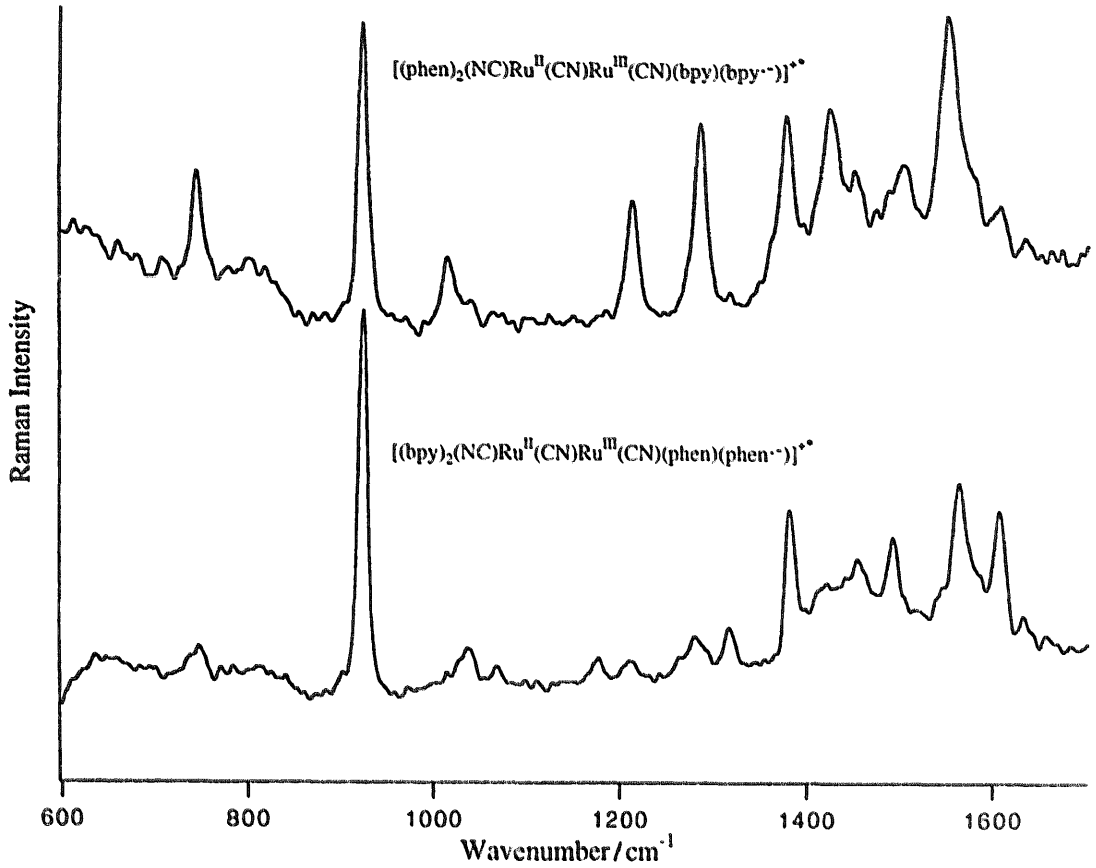

Fig. 5. Transient resonance Raman spectra (600–1700 cm^{-1}) of $[(NC)(phen)_2Ru(CN)Ru(bpy)_2(CN)]^{2+*}$ and $[(NC)(bpy)_2Ru(CN)Ru(phen)_2(CN)]^{2+*}$ at similar concentrations and experimental conditions as in Fig. 2.

only $phen^{\bullet-}$ enhancements are observed. These observations are consistent with facile, cross-bridge energy transfer [28].

Resonance Raman measurements have also been used to demonstrate that protonation, to give $[(NC)(phen)_2Ru(CN)Ru(bpy)_2(CNH)]^{2+}$, reverses the direction of energy transfer [29]. Protonation converts the terminal cyanide into a strongly backbonding isocyanide ligand. This increases the energy of the lowest $Ru^{III}(bpy^{\bullet-})$ MLCT state and inverts the ordering of the lowest $Ru^{III}(bpy^{\bullet-})$ and $Ru^{III}(phen^{\bullet-})$ states.

In the dibridged complex, $[(NC)(bpy)_2Ru(CN)Ru(4,4'\text{-}(CO_2H)_2bpy)_2(NC)Ru(bpy)_2(CN)]^{2+}$ ($4,4'\text{-}(CO_2H)_2bpy$ is 4,4′-$(CO_2H)_2$-2,2′-bipyridine), the carboxylic acid groups provide sites for binding the central Ru to the surface of TiO_2 semiconductor electrodes. Excitation of the terminal sites is followed by rapid energy transfer to the center giving the lowest-energy MLCT excited state at the center. This state injects an electron into the conduction band of TiO_2. The net effect is visible sensitization of the semiconductor [26]. In regenerative photoelectrochemical cells with this complex on nanocrystalline TiO_2, 400- to 700-nm photons are converted into electrons with high efficiencies.

Time-resolved resonance Raman studies on $[(NC)(bpy)_2Ru(CN)$

$Ru(4,4'-(CO_2^-)_2bpy)_2(NC)Ru(bpy)_2(CN)]^{2-*}$ have been used to demonstrate that energy transfer does occur in solution [30]. The bands that appear in the excited state spectrum are those of the dicarboxy ligand.

The cyano-bridging chemistry has been extended to the oligomers $[(phen)(CO)_3Re(CN)[Ru(bpy)_2(CN)]_nRu(bpy)_2]^{(n+1)+}$ ($n=0$, 1, 2, 3). In this series, each Ru^{II} unit is bridged by two cyanides. One is carbon-bound and the other nitrogen-bound. In the oligomers there is a built-in free energy gradient that drives an intramolecular energy transfer cascade (Scheme 6). The ordering of excited-state energies in the cascade is: $Re^{II}(phen^{\cdot -}) > Ru^{III}(bpy^{\cdot -})_{bridge} > Ru^{III}(bpy^{\cdot -})_{terminal}$. For $n=2,3$, $Re^{I} \rightarrow phen$ excitation to give the $Re^{II}(phen^{\cdot -})$ excited state is followed by rapid (<1 ns) energy transfer to a bridge unit. Once on a bridge unit further energy transfer can occur by $Ru^{III}(bpy^{\cdot -})_{bridge} \rightarrow Ru^{III}(bpy^{\cdot -})_{bridge}$ energy transfer hopping or which $\Delta G^0 \sim O$. This is the mechanism that leads to long-range energy transfer, Scheme 6.

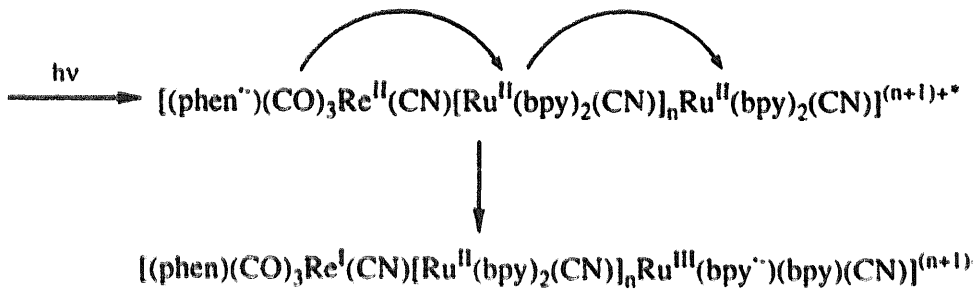

Scheme 6.

Within experimental error, the same emission lifetimes are found for the oligomers with $n=1-3$ consistent with rapid energy transfer to the terminal $Ru^{III}(bpy)$ unit. Transient Raman measurements were used to obtain direct evidence for energy transfer [27]. In Fig. 6 are shown transient spectra for $[(phen)(CO)_3Re(NC)Ru(bpy)_2(CN)]^{+*}$, $[(phen)(CO)_3Re(NC)Ru(phen)_2(CN)]^{+*}$ and $[(phen)(CO)_3Re(NC)Ru(phen)_2(CN)Ru(bpy)_2(CN)]^{2+*}$ in CH_3CN. For $[(phen)(CO)_3Re(NC)Ru(bpy)_2(CN)]^{+}$, simultaneous $Re^{I} \rightarrow phen$, $Ru^{II} \rightarrow bpy$ excitation results only in enhanced $bpy^{\cdot -}$ bands. Only enhanced $bpy^{\cdot -}$ bands are observed for $[(phen)(CO)_3Re(NC)Ru(phen)_2(CN)Ru(bpy)_2(CN)]^{2+}$. Both observations are consistent with energy transfer to the terminal Ru within the laser pulse (<10 ns).

3. Time-resolved infrared

3.1. Background

The application of time-resolved infrared spectroscopy opens new vistas for exploring excited state molecular and electronic structure in transition metal complexes.

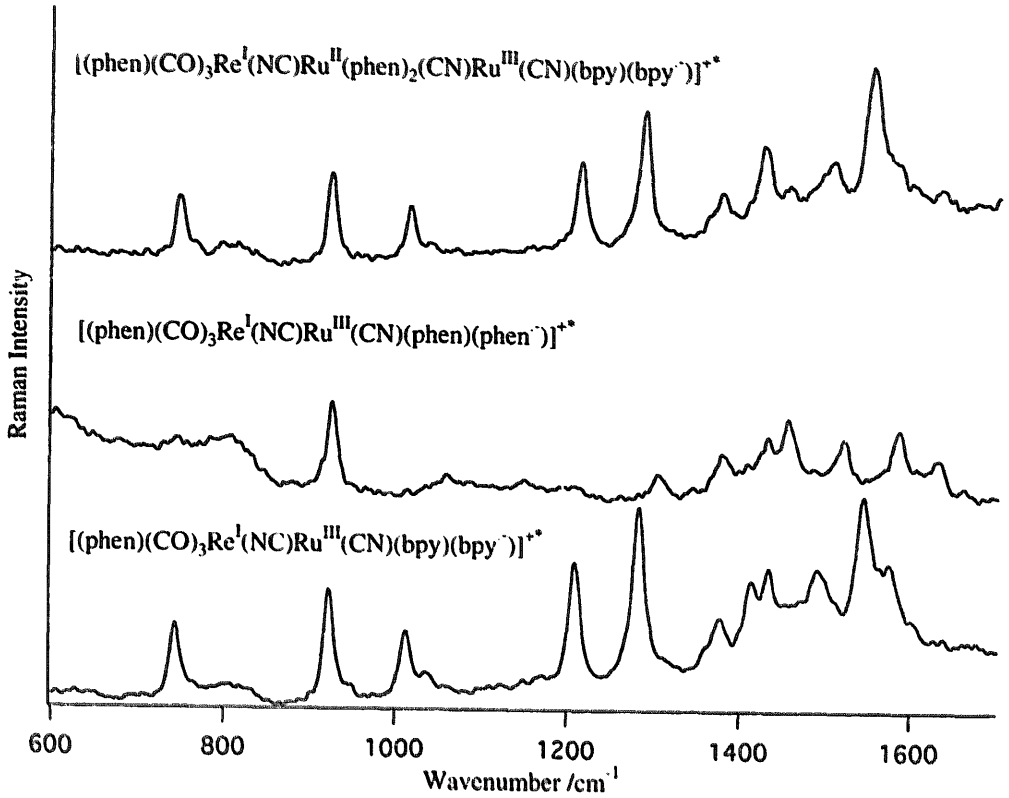

Fig. 6. Transient resonance Raman spectra for $[(phen)(CO)_3Re(NC)Ru(bpy)_2(CN)]^{+*}$, $[(phen)(CO)_3Re(NC)Ru^{II}(phen)_2(CN)]^{+*}$ and $[(phen)(CO)_3Re(NC)Ru(phen)_2(CN)Ru(bpy)_2(CN)]^{2+*}$ measured in CH_3CN at room temperature, as in Fig. 2.

The first polypyridyl example came from Turner's work on $[Re(4,4'\text{-bpy})_2(CO)_3Cl]$ (4,4'-bpy is 4,4'-bipyridine) [30]. These and other transient infrared results have appeared in a recent review [3]a.

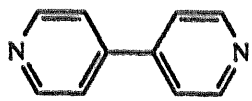

4,4'-bpy

3.2. Instrumentation

Continuing advances in instrumentation have led to the ability to measure transient infrared spectra following laser excitation on a variety of timescales. Initial experiments on the nanosecond timescale utilized a monochromatic monitoring beam and a pulsed laser excitation source with transient signals monitored point by point over the spectral region of interest. A new and more versatile approach utilizes step-scan Fourier transform interferometry [31]. In the step-scan interferometer, the mirror is held at a fixed position while a transient is produced by pulsed laser excitation.

The moving mirror is stepped to a second position and the process repeated. Temporal digitization following the laser pulse is synchronized with each discrete mirror position. The temporal resolution that can be achieved is limited by the detector response time, the digitization rate or the laser pulse width. Spectral resolution and range are determined by the number and interval between steps. Once acquired, the data are recast by a control computer to yield interferograms at a sequence of times. Fourier transformation yields time-resolved spectra and an absorbance–time map of the temporal evolution of the spectrum.

For measurements on the nanosecond time scale, it is possible to modify commercial instrumentation to study short-lived excited states and intermediates as shown in Fig. 7; the infrared beam from the step-scan interferometer is directed out of a sampling port to a mirror (M1) which directs the light to lens L1. This lens tightly focuses (to a ~500 μm spot diameter) the infrared light onto the sample. The pump beam from a Q-switched Nd:YAG laser operating at 10 Hz is introduced at a small angle relative to the probe beam. The infrared light is collected by lens L2 and focused by L3 onto the element of a photoconductive mercury cadmium telluride (MCT) detector. A low-pass germanium optical filter at 2250 cm^{-1} is attached to the face of the MCT detector to block visible or near-infrared emission from the sample and to increase the dynamic range of the detector by filtering infrared light outside the region of interest. The filter, CaF_2 cell windows and CaF_2 optics (high-pass 1250 cm^{-1}) provide the spectral region of 1250 to 2250 cm^{-1}. The optical system is contained in a Plexiglas enclosure purged with dry nitrogen.

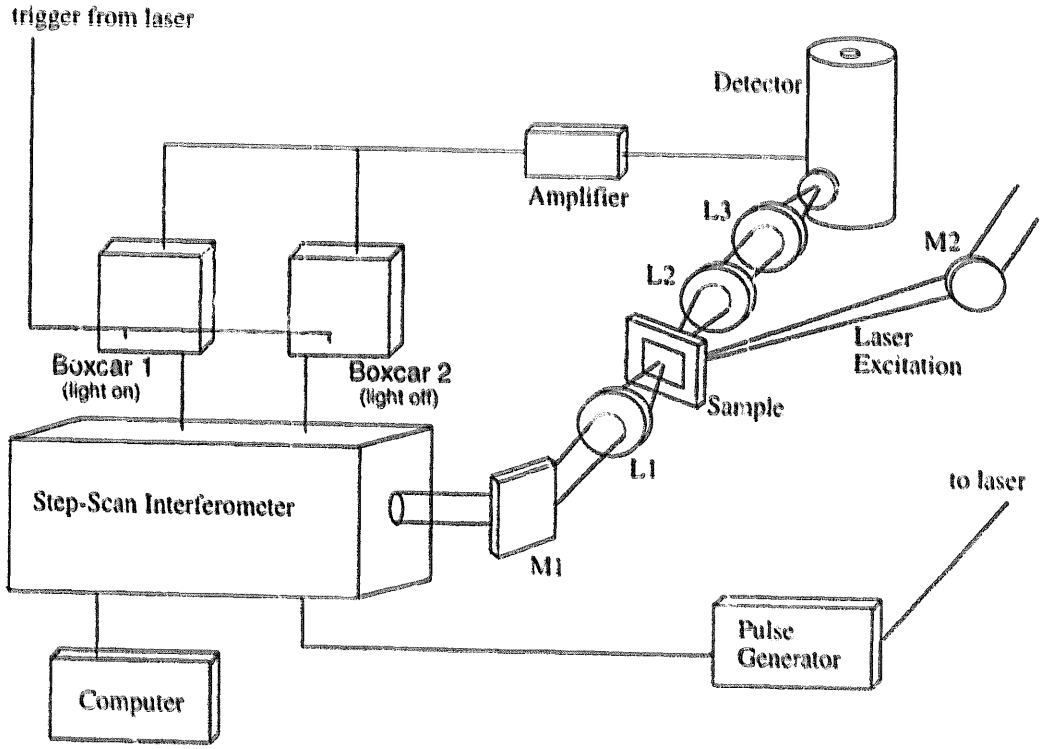

Fig. 7. Schematic diagram for a time-resolved, step-scan Fourier transform infrared difference spectrometer as described in the text.

The pump–probe approach can also be used to measure ultrafast infrared spectra. In one experiment short infrared pulses are used as the probe beam based on a picosecond or femtosecond laser system [3]b. The probe beam is split into sample and reference beams before excitation of the sample. The difference in response is measured by a mid-infrared sensitive detector.

3.3. Applications

3.3.1. Electronic structure of excited states

The time-resolved technique has been successfully applied to the elucidation of electronic structure and excited state ordering in CO-containing polypyridyl complexes of Re^{I} [32]. A complex interplay between MLCT and ligand-based excited states is known to exist in these complexes [33].

Ground-state and transient infrared difference spectra for *fac*-$[Re(phen)(CO)_3(4\text{-Mepy})]^+$ (4-Mepy is 4-Methylpyridine) in the ν(CO) region are shown in Fig. 8a. The difference spectrum was measured following 354.7 nm excitation in CH_3CN by using step-scan interferometry. In this spectrum, the broad, ground-state ν(CO) band at 1931 cm^{-1} appears as a bleach with new excited-state bands appearing at 1965 and 2015 cm^{-1} [31,32]. The broad band in the ground state actually consists of two overlapping ν(CO) bands. They are resolved in the excited state because reduction at phen to give $phen^{\cdot -}$ decreases the local electronic symmetry. In the ground state the three facial pyridyl-type ligands (4-Mepy and the two pyridyl rings of phen) are electronically similar. In the MLCT excited state phen becomes $phen^{\cdot -}$, distinct from 4-Mepy. The third ν(CO) band at 2036 cm^{-1} also shifts to higher energy (2065 cm^{-1}) in the excited state. The shifts to higher energy are consistent with partial oxidation of Re^{I} to Re^{II} and formation of the $Re^{II}(phen^{\cdot -})$ excited state. The energies of the ν(CO) bands increase because of the decrease in Re–CO backbonding to Re^{II}. This increases the triple bond character of the CO ligands. Related observations have been made following MLCT excitation of $[Re(bpy)(CO)_3(4\text{-Etpy})]^+$ (4-Etpy is 4-Ethylpyridine) and $[Re(4,4'\text{-bpy})_2(CO)_3(Cl)]^+$ (4,4′-bpy is 4,4′-bipyridine) [3]a,e.

The increase in ν(CO) is a general effect. MLCT excitation of $[Os(tpy)(bpy)(CO)]^{2+}$ (tpy is 2,2′:6′,2″-terpyridine) in CH_3CN (Fig. 9) results in a shift in ν(CO) from 1974 to 2044 cm^{-1} with $\Delta\nu(CO) = +70\ cm^{-1}$. The shift is $+73\ cm^{-1}$ for $[Os(phen)_2(CO)Cl]^+$ and $+69\ cm^{-1}$ for $[Os(bpy)_2(CO)(pyridine)]^{2+}$ [34].

The transient infrared difference spectrum for *fac*-$[Re(dppz)(CO)_3(PPh_3)]^{+*}$ (dppz is dipyrido[3,2-*a*:2′,2′-*c*]phenazine; PPh_3 is triphenylphosphine) is shown in Fig. 8b. In this case the three ν(CO) bands in the excited state are only slightly shifted and the shifts are to *lower* energy. The transient spectrum can be simulated qualitatively by assuming that the ν(CO) bands in the excited state are slightly broadened and decreased in energy by ca. 5 cm^{-1} in the excited state. There is no evidence for bands at higher energy characteristic of a MLCT excited state. A similar result was obtained for *fac*-$[Re(dppz)(CO)_3(4\text{-Etpy})]^+$.

The relatively small shifts in ν(CO) in the dppz complexes are consistent with a

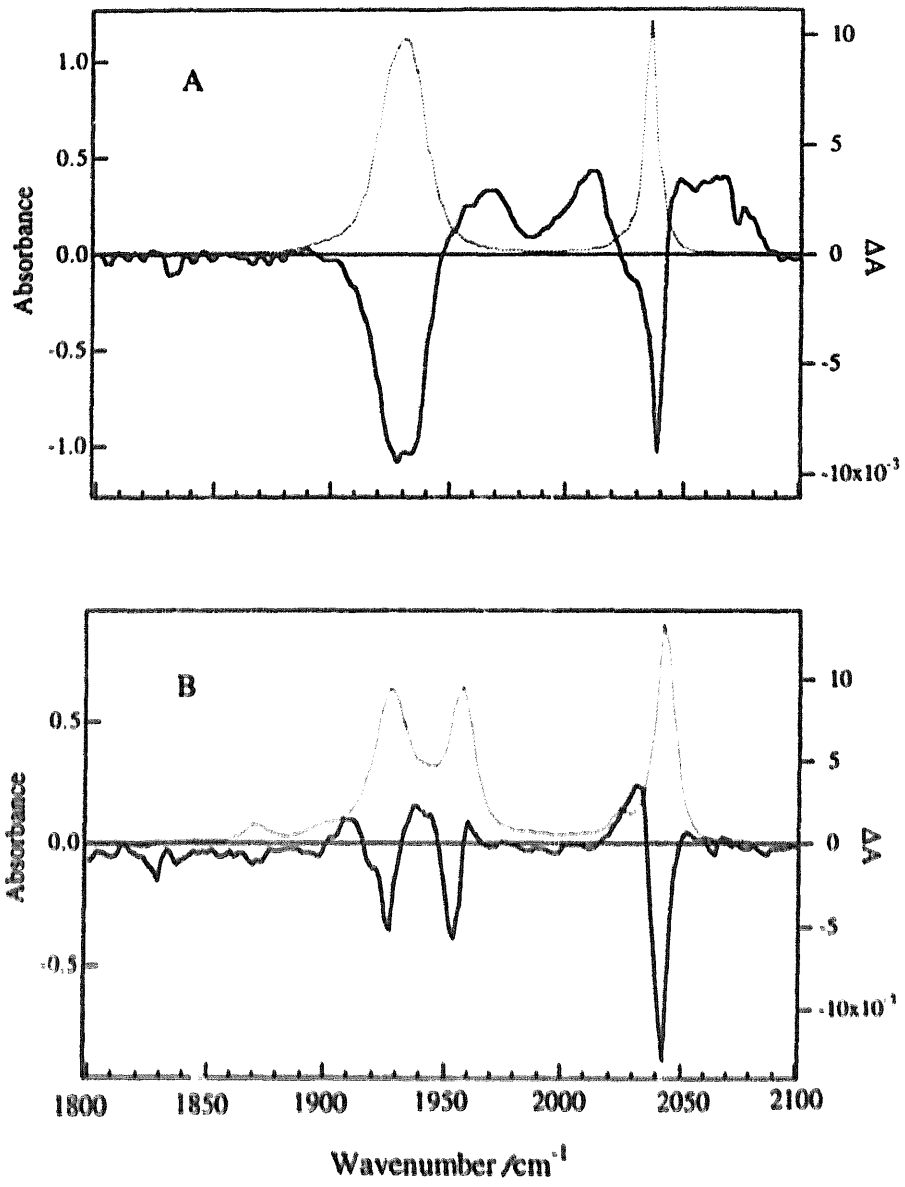

Fig. 8. Ground-state (broken curve) and 600 ns time-resolved infrared difference spectra of *fac*-[Re(phen)(CO)$_3$(4-Mepy)]$^+$ (phen is 1,10-phenanthroline; 4-Mepy is 4-methylpyridine) (a) compared to *fac*-[Re(dppz)(CO)$_3$(PPh$_3$)]$^+$ (dppz is dipyrido[3,2-*a*:2',3'-*c*]phenazine; PPh$_3$ is triphenylphosphine) (b). Excitation was at 354.7 nm with a sample concentration of ca. 1 mM in CH_3CN at room temperature.

ligand-localized excited state which is slightly electron donating at the metal relative to ground-state dppz. For the dppz complex this is a lowest-lying, dppz-based $^3\pi\pi^*$ state. Room temperature emission spectra and lifetimes identify this state by its long lifetime (15 μs) and characteristic $\pi\pi^*$ vibronic progressions [35].

Replacement of 4-Etpy or PPh$_3$ by Cl^- in *fac*-[Re(dppz)(CO)$_3$Cl] results in a dramatic change in excited-state properties at room temperature. A broad MLCT emission appears with $\tau = 25$ ns (CH_3CN at 298 K). The substitution of electron donating Cl^- for 4-Etpy or PPh$_3$ stabilizes the Re^{II}(dppz$^{\cdot-}$) MLCT state sufficiently that it is thermally populated at room temperature and dominates excited-state

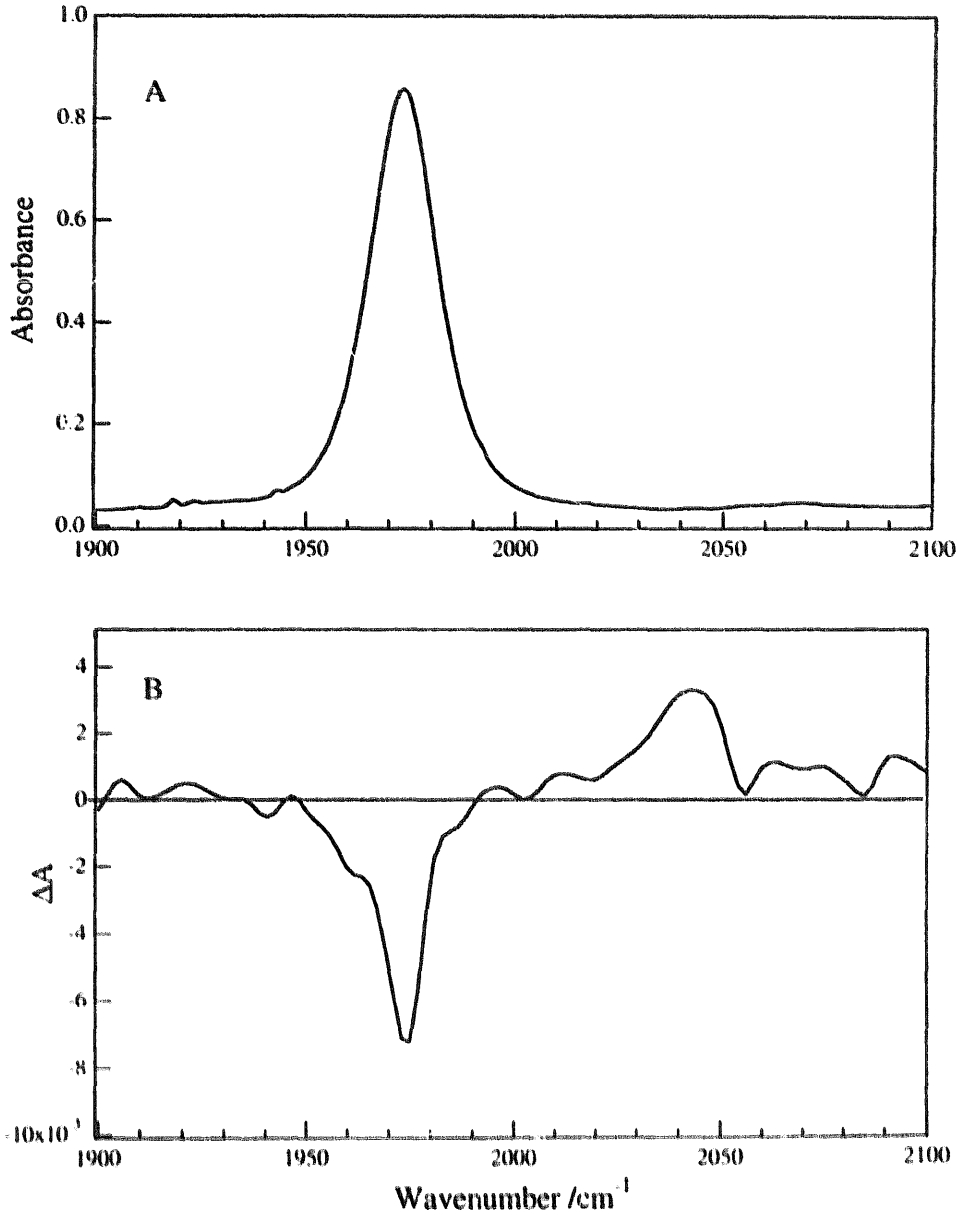

Fig. 9. Ground-state (a) and time-resolved infrared difference spectra (b) measured following 354.7 nm excitation for $[Os(tpy)(bpy)CO]^{2+}$ (tpy is 2,2′: 6′,2″-terpyridine) in CH_3CN at room temperature.

decay at room temperature. The ππ* (dppz) state is still lowest lying and the only emitter at low temperature.

The utility of the transient infrared technique to elucidate electronic structure is further illustrated by measurements on *fac*-[Re(4,4′-$(NH_2)_2$bpy)$(CO)_3$(4-Etpy)]$^+$ (4,4′-$(NH_2)_2$bpy is 4,4′-diamino-2,2′-bipyridine). When excited in fluid solution, this complex is a characteristic MLCT emitter with a broad, short-lived ($\tau = 280$ ns) emission at $\lambda_{max} = 570$ nm in 2-methyltetrahydrofuran at 298 K [36]. In transient absorption difference spectra, there is evidence for more than one state with a broad absorption feature centred at 450 nm and a narrow feature at

370 nm. The relative intensities of the two are both solvent and temperature dependent [36].

In Fig. 10 is shown the transient infrared difference spectrum of *fac*-[Re(4,4'-$(NH_2)_2$)bpy)$(CO)_3$(4-Etpy)]$^+$. The features that appear can be explained by invoking a MLCT excited state which co-exists with at least one, and perhaps two, ligand-based states. Further elucidation of this obviously complex system will require additional measurements as a function of temperature. Gaussian fitting of the data in Fig. 10 reveals a set of positively shifted ν(CO) bands with shifts for a MLCT state comparable to *fac*-[Re(phen)$(CO)_3$(4-Mepy)]$^{+*}$. Another set of bands can be found in the spectrum which are slightly shifted to lower energy reminiscent of *fac*-[Re(dppz)$(CO)_3(PPh_3)]^{+*}$. There is evidence for still a third set of bands slightly shifted to higher energy. The state responsible for these bands may be a ligand-based $n\pi^*$ state.

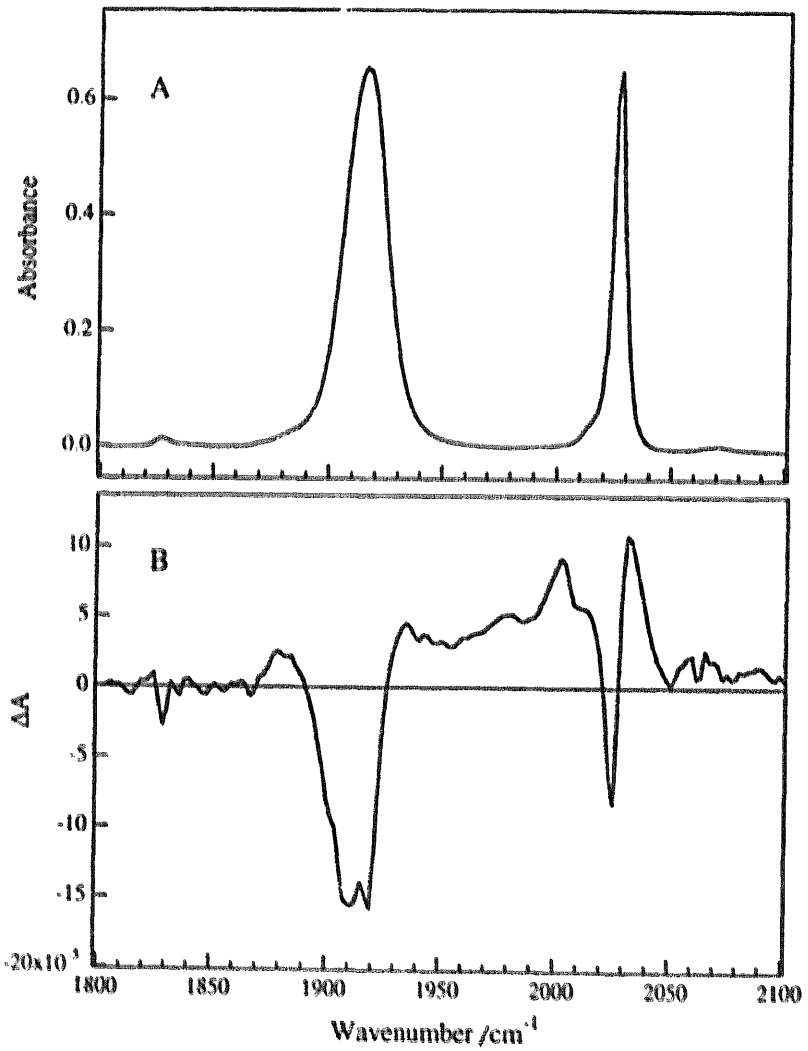

Fig. 10. Ground-state (a) and 600 ns time-resolved infrared difference spectra (b) for *fac*-[Re(4,4'-$(NH_2)_2$(bpy)$(CO)_3$(4-Etpy)]$^+$ (4,4'-$(NH_2)_2$)bpy is 4,4'-diamino-2,2'-bipyridine) in CH_3CN at room temperature following 354.7 nm excitation.

Transient infrared measurements have also been used to reveal co-existing excited states in the ligand-bridged complex $[(4\text{-Etpy})(CO)_3Re^{I}(\mu\text{-bbpe})Re^{I}(CO)_3(4\text{-Etpy})]^{2+}$. Following $Re^{I}\rightarrow$bbpe excitation at 354.7 nm, characteristic ν(CO) bands are observed for both $\pi\pi^*$ and MLCT excited states [11]e.

3.3.2. *Intramolecular energy transfer*

A common structural motif in many molecular assemblies based on polypyridyl complexes is ligand bridging. The use of ligand bridges provides a ready basis for fabricating complex oligomeric assemblies. The increased complexity of the molecular architecture in these systems further complicates analysis of excited-state properties. In the previous section, transient Raman measurements and chemical synthesis were combined to study energy transfer in cyano-bridged complexes. The same identification of intermediates can be made by transient infrared measurements on a single sample by monitoring changes in ν(CO) or ν(CN) bands. As seen in the examples above, they can provide a direct probe of metal oxidation state.

In transient infrared spectra following MLCT excitation of $[(NC)(bpy)_2Ru(CN)Ru(phen)_2(CN)]^{+}$, the ground-state cyanide band at 2079 cm^{-1} is bleached and excited-state bands appear at 2037, 2091 and 2104 cm^{-1} [31,37]. The remaining ground-state bleach near 2101 cm^{-1} is masked by excited-state bands in this region. Comparison of the spectrum with that of the mixed-valence ion $[(NC)(bpy)_2Ru^{II}(CN)Ru^{III}(bpy)_2(CN)]^{2+}$, prepared by chemical oxidation, demonstrates that the excited state is best described as $[(NC)(bpy)_2Ru^{II}(CN)Ru^{III}(phen)(phen^{\cdot -})(CN)]^{+*}$ with the lowest MLCT excited state at the N-bonded chromophore. Although significant electronic coupling exists across the CN^{-} bridge, the transient spectroscopic results are consistent with localized Ru^{III} and Ru^{II} and separate, localized MLCT excited states.

The ligand-bridged complex $[(phen)(CO)_3Re(NC)Ru(bpy)_2(CN)]^{+}$ was the parent molecule in the study of long-range energy transfer in a previous section. It possesses two absorbing chromophores in the visible, $Ru^{II}\rightarrow$bpy with $\lambda_{max}=450$ nm and $Re^{I}\rightarrow$phen at 380 nm. Transient resonance Raman studies on the ns time scale reveal that rapid $Re^{II}(phen^{\cdot -})\rightarrow Ru^{II}(bpy)$ energy transfer occurs following $Re^{I}\rightarrow$phen excitation. Transient infrared measurements reinforce this conclusion. In the infrared spectrum of the ground state in CH_3CN, ν(CO) bands appear at 1920 and 2028 cm^{-1}, the terminal ν(CN) stretch at 2081 cm^{-1}, and ν(CN) for the bridge at 2100 cm^{-1}. In spectra measured 400 ns after 354.7 nm excitation, the terminal ν(CN) shifts from 2081 to 2108 cm^{-1} and the bridge ν(CN) from 2100 to 2132 cm^{-1}, Fig. 11C. The shifts in ν(CO) are small ($\Delta\nu$(CO) ~ 5 cm^{-1}) compared to the large shifts for $Re^{II}(bpy^{\cdot -})$ MLCT states. These observations are consistent with the appearance of oxidation states Re^{I} and Ru^{III} in the transient intermediate formed by laser flash photolysis on the ns time scale. They also demonstrate that rapid $Re^{II}(phen^{\cdot -})\rightarrow Ru^{II}(bpy)$ energy transfer occurs following $Re^{I}\rightarrow$phen excitation, Scheme 7.

Ultrafast transient infrared measurements on the picosecond timescale provide additional insight and direct evidence for the initial $Re^{II}(phen^{\cdot -})$ excited state in Scheme 7 [3]e. Early time features acquired ~1 ps after laser flash excitation at

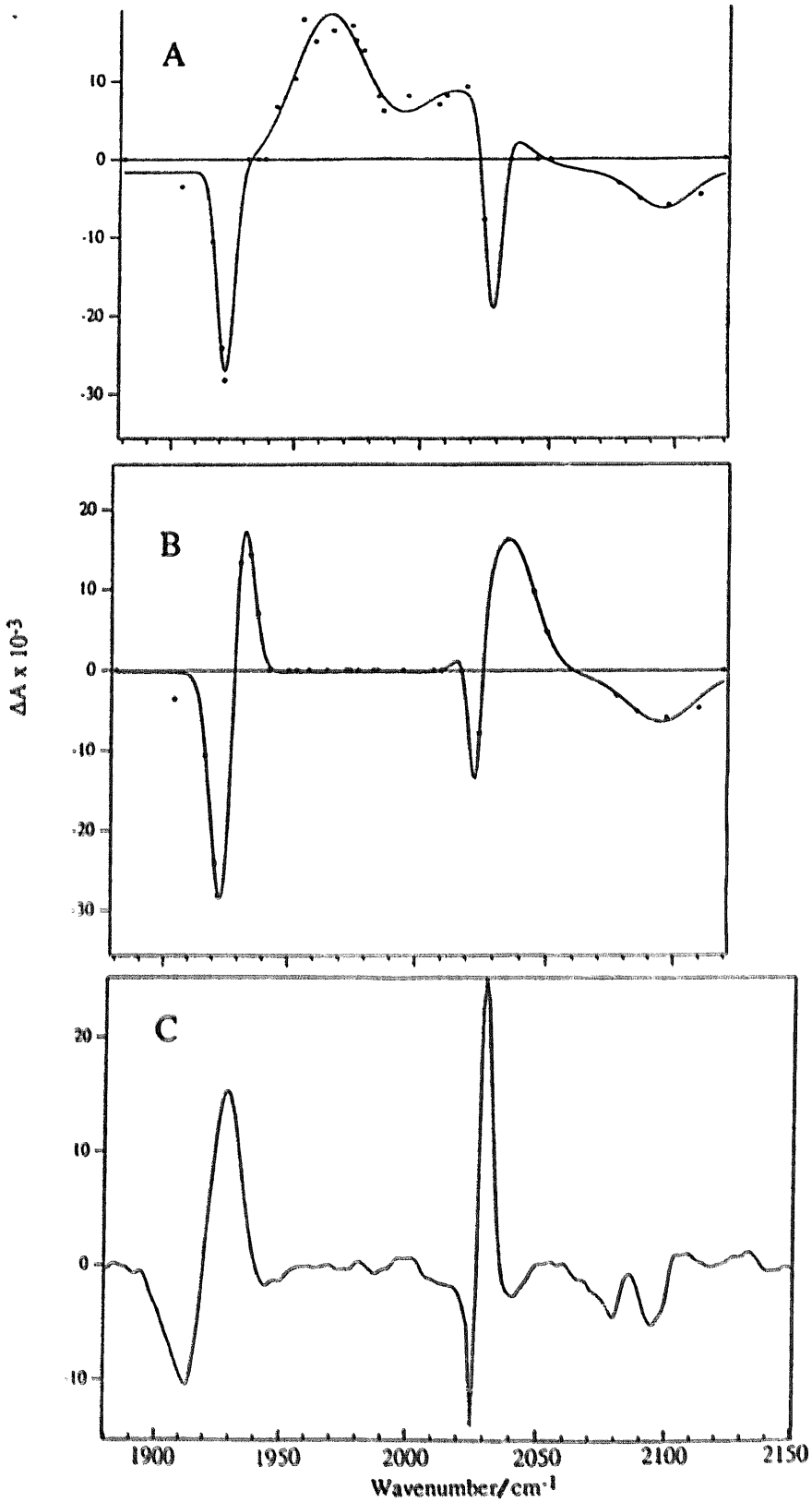

Fig. 11. Comparison of nanosecond transient infrared spectra of $[(phen)(CO)_3Re(NC)Ru(bpy)_2(CN)]^+$ (c) compared to the 1 ps (a) and 40 ps (b) time-resolved infrared spectra as in Fig. 8.

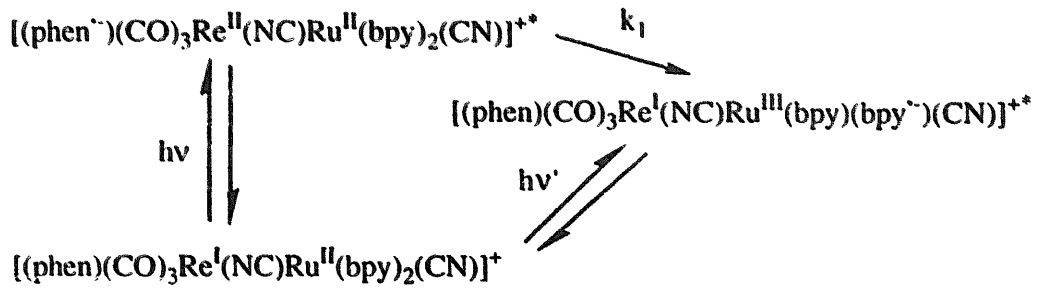

Scheme 7.

300 nm resemble those of a typical MLCT state (Fig. 11a). Ground-state bleaches near 1930 and 2030 cm^{-1} are observed with positive shifts in ν(CO) in the excited state. These features decay in 5 ps. The transient spectrum after 40 ps (Fig. 11b) is very similar to the spectrum observed in the ns study suggesting that after 40 ps, [(phen)(CO)$_3$Re^{I}(NC)Ru^{III}(bpy$^{\cdot-}$)(bpy)(CN)]$^{+*}$ is nearly fully formed. Analysis of the time dependent data shows that these features appear in 10 ps. The details of the transition between states remain to be properly defined. Simple Re^{II}(phen$^{\cdot-}$)→Ru^{II}(bpy) energy transfer does not explain the difference in the appearance and disappearance kinetics. The most plausible explanation is that there is an intermediate state. A reasonable mechanism is energy transfer by sequential electron transfer, first from Ru^{II} to Re^{II}, [(phen$^{\cdot-}$)(CO)$_3$ Re^{II}(NC)Ru^{II}(bpy)$_2$(CN)]$^{+*}$→[(phen$^{\cdot-}$)(CO)$_3$Re^{I}(NC)Ru^{III}(bpy)$_2$(CN)]$^{+*}$, followed by phen$^{\cdot-}$ to bpy, [(phen$^{\cdot-}$)(CO)$_3$Re^{I}(NC)Ru^{III}(bpy)$_2$(CN)]$^{+*}$→ [(phen)(CO)$_3$Re^{I}(NC)Ru^{III}(bpy$^{\cdot-}$)(bpy)(CN)]$^{+*}$. Ultrafast infrared studies are currently being undertaken to establish additional details about this reaction.

4. Conclusions

The results reviewed here demonstrate that transient vibrational spectroscopies can be powerful tools for elucidating electronic and molecular structure of excited states and photochemical intermediates. When combined and applied on various timescales, time-resolved resonance Raman and infrared add significantly to the information that can be obtained by more conventional transient emission and absorption measurements. They are especially useful in identifying intermediates based on Raman fingerprinting and infrared shifts in ν(CO) and ν(CN) bands in metal complexes. With greater knowledge of normal coordinates and the effects of electron density on the energies of vibrational bands, they will become important tools for calculating, or at least inferring, excited-state structure.

Further developments in instrumentation will have an important impact on advances in this area. The ability to use the time-resolved, step-scan Fourier transform technique on the 10's of ns timescale simplifies data collection and allows data to be collected throughout the infrared. Transient infrared studies will no longer be limited to complexes containing CO or CN^- ligands. Advances in detector

technology will allow even relatively weak bands to be observed and more dilute solutions to be used to make measurements. Continued application of ultrafast measurements will open new opportunities for studying fundamental processes at very early times. Because of their sensitivity to structural change, they will give unprecedented insight into these early time events.

These techniques will continue to be of great value in elucidating the role of structure and defining transient photochemical electron and energy transfer in molecular assemblies. When combined with transient absorption and emission measurements, they provide a means for acquiring the broad set of experimental information required to answer detailed questions about mechanism and structure.[21]

Acknowledgements

Support from DOE (Grant DE-FG05-86ER13633) and NSF (Grant CHE-9321413) to T.J.M. at UNC are acknowledged. Part of this work was performed at Los Alamos National Laboratory under the auspices of the U.S. Department of Energy. Support from the Laboratory Directed Research and Development Program to J.R.S. is also acknowledged. We thank Drs. W. Douglas Bates and Geoffrey Strouse for their input.

References

[1] (a) T.J. Meyer, Accts. Chem. Res. 22 (1989) 163; (b) R. Scandola, M.T. Indelli, C. Chiorboli, C.A. Bignozzi, Topics Curr. Chem. 158 (1990) 73; (c) V. Balzani, F. Scandola, Supramolecular Photochemistry, Horwood, Chichester, UK, 1991, ch. 5 and 6; (d) K. Kalyanasundaram, Photochemistry of Polypyridine and Porphyrin Complexes, Academic Press, London, 1992.

[2] (a) D.E. Morris, W.H. Woodruff, in: R.J.H. Clark, R.E. Hester (Eds.), Spectroscopy of Inorganic-based Materials, John Wiley and Sons, New York, 1987; (b) C.V. Kumar, J.K. Barton, N.J. Turro, I.R. Gould, Inorg. Chem. 26 (1987) 1455; (c) D.S. Caswell, T.G. Spiro, Inorg. Chem. 26 (1987) 18; (d) C.V. Kumar, J.K. Barton, I.R. Gould, N.J. Turro, J.V. Houten, Inorg. Chem. 27 (1988) 648; (e) T. Yabe, D.R. Anderson, L.K. Orman, Y.S. Chang, J.B. Hopkins, J. Phys. Chem. 93 (1989) 2302; (f) Y.S. Chang, X. Xu, T. Yave, S.-C. You, D.R. Anderson, L.K. Orman, J.B. Hopkins, J. Phys. Chem. 94 (1990) 729; (g) T. Yabe, L.K. Orman, D.R. Anderson, S.-C. Yu, X. Xu, J.B. Hopkins, J. Phys. Chem. 94 (,990) 7128; (h) G.D. Danzer, J.R. Kincaid, J. Phys. Chem. 94 (1990) 3976; (i) C. Turro, S.H. Bossmann, G.E. Leroi, J.K. Barton, N.J. Turro, Inorg. Chem. 33 (1994) 1344; (j) M.T. Indelli, C.A. Bignozzi, A. Harriman, J.R. Schoonover, F. Scandola, J. Am. Chem. Soc. 116 (1994) 3768; (k) S.M. Treffert-Ziemelis, J. Golus, D.P. Strommen, J.R. Kincaid, Inorg. Chem. 32 (1993) 3890; (l) K.C. Gordon, J.J. McGarvey, Inorg. Chem. 30 (1991) 2986; (m) K.C. Gordon, J.J. McGarvey, Chem. Phys. Lett. 173 (1990) 443; (n) D.P. Strommen, P.K. Mallick, G.D. Danzer, R.S. Lumpkin, J.R. Kincaid, J. Phys. Chem. 94 (1990) 1357; (o) G.D. Danzer, J.A. Golus, J.R. Kincaid, J. Am. Chem. Soc. 115 (1993) 8643.

[3] (a) J.J. Turner, M.W. George, F.P.A. Johnson, J.R. Westwell, Coord. Chem. Rev. 125 (1993) 101; (b) P.O. Stoutland, R.B. Dyer, W.H. Woodruff, Science 257 (1992) 1913; (c) R.M. Hochstrasser, P.A. Anfinrud, R. Diller, C. Han, M. Iannone, T. Lian, B. Locke, in: Ultrafast Phenomena VII, 1990, 229; (d) R.A. Palmer, Spectroscopy 8 (1993) 26; (e) J.R. Schoonover, K.C. Gordon, R. Argazzi, W.H. Woodruff, K.A. Peterson, C.A. Bignozzi, R.B. Dyer, T.J. Meyer, J. Am. Chem. Soc. 115 (1993) 10 996.

[4] (a) D.A. Long, Raman Spectroscopy, McGraw–Hill, London, 1977; (b) K. Nakamoto, Infrared and Raman Spectra of Inorganic and Coordination Complexes, 4th ed., Wiley and Sons, New York, 1986.
[5] (a) A.C. Albrecht, J. Chem. Phys. 34 (1961) 1476; (b) A.C. Albrecht, M.C. Hutley, J. Chem. Phys. 55 (1971) 4438.
[6] (a) E.J. Heller, Acc. Chem. Res. 14 (1981) 368; (b) E.J. Heller, R.L. Sunberg, D.J. Tannor, J. Phys. Chem. 86 (1982) 1822.
[7] R.F. Dallinger, W.H. Woodruff, J. Am. Chem. Soc. 101 (1979) 4391.
[8] (a) J. McClanahan, R.F. Dallinger, F.J. Holler, J.R. Kincaid, J. Am. Chem. Soc. 107 (1985) 4853; (b) P.A. Mabrouk, M.S. Wrighton, Inorg. Chem. 25 (1986) 526.
[9] G.F. Strouse, P.A. Anderson, J.R. Schoonover, T.J. Meyer, F.R. Keene, Inorg. Chem. 31 (1993) 3004.
[10] S. Boyd, G.F. Strouse, W.E. Jones, Jr., T.J. Meyer, J. Am. Chem. Soc. 112 (1990) 7395.
[11] (a) R.P. Van Duyne, M.R. Suchanski, J.M. Lakovits, A.R. Siedle, K.D. Parks, T.M. Cotton, J. Am. Chem. Soc. 101 (1979) 2832; (b) D.C. Jeanmarie, R.P. Van Duyne, J. Am. Chem. Soc. 98 (1976) 4029; (c) F.W. Langkilde, R. Wilbrandt, F. Negri, G. Orland, Chem. Phys. Lett. 165 (1990) 66; (d) G.F. Strouse, Ph.D. dissertation, The University of North Carolina, Chapel Hill, 1993; (e) G.F. Strouse, J.R. Schoonover, R. Duesing, T.J. Meyer, Inorg. Chem. 34 (1995) 2725.
[12] (a) E. Amouyal, A. Homsi, J.-C. Chambron, J.-P. Sauvage, J. Chem. Soc., Dalton Trans. (1990) 1841; (b) J.-C. Chambron, J.-P. Sauvage, E. Amouyal, P. Koffi, Nouv. J. Chim. 9 (1985) 547; (c) M.N. Ackermann, L.V. Interrante, Inorg. Chem. 23 (1984) 3904.
[13] R.E. Hester, K.P.J. Williams, J. Raman Spec. 13 (1982) 91.
[14] (a) G.D. Danzer, J.A. Golus, J.R. Kincaid, J. Am. Chem. Soc. 115 (1993) 8643; (b) S.M. Treffert-Ziemelis, J.A. Golus, D.P. Strommen, J.R. Kincaid, Inorg. Chem. 32 (1993) 3892; (c) S.M. Treffert-Ziemelis, J.R. Kincaid, J. Raman Spectrosc. 25 (1994) 893.
[15] (a) P. Chen, E. Danielson, T.J. Meyer, J. Phys. Chem. 92 (1988) 3708; (b) T.D. Westmoreland, H. LeBozec, R.W. Murray, T.J. Meyer, J. Am. Chem. Soc. 105 (1983) 5952; (c) P. Chen, T.D. Westmoreland, E. Danielson, K.S. Schanze, D. Anthon, P.E. Neveux, T.J. Meyer, Inorg. Chem. 26 (1987) 1116; (d) P. Chen, R. Duesing, G. Tapolsky, T.J. Meyer, J. Am. Chem. Soc. 111 (1989) 8305; (e) K.S. Schanze, K. Sauer, J. Am. Chem. Soc. 110 (1988) 1180; (f) D.B. MacQueen, K.S. Schanze, J. Am. Chem. Soc. 113 (1991) 7470; (g) L.S. Fox, M. Kozik, J.R. Winkler, H.B. Gray, Science, 247 (1990) 1069; (h) S.L. Carson, L.F. Cooley, C.M. Elliot, D.F. Kelley, J. Am. Chem. Soc. 114 (1992) 9504; (i) T.J. Meyer, in: N. Kitamura (Ed.), Photochemical Processes in Organized Molecular Systems, Elsevier, Amsterdam, 1991, p. 133; (j) Photoinduced Electron Transfer I–3, J. Mattey (Ed.), Top Curr. Chem. (1990) (1991) 156, 158, 159; (k) Photoinduced Electron Transfer, M.A. Fox, M. Chanon (Eds.), Elsevier, New York, 1988.
[16] J.R. Schoonover, P. Chen, W.D. Bates, T.J. Meyer, Inorg. Chem. 33 (1994) 793.
[17] (a) P.G. Bradley, N. Kress, B.A. Hornberger, R.F. Dallinger, W.H. Woodruff, J. Am. Chem. Soc. 103 (1981) 7441; (b) W.K. Smothers, M.S. Wrighton, J. Am. Chem. Soc. 105 (1983) 1067; (c) P.K. Mallick, D.P. Strommen, J.R. Kincaid, J. Am. Chem. Soc. 112 (1990) 1686; (d) P.K. Mallick, G.D. Danzer, D.P. Strommen, J.R. Kincaid, J. Phys. Chem. 92 (1988) 5628.
[18] C. Takahashi, S. Maeda, Chem. Phys. Lett. 24 (1974) 585.
[19] R.E. Hester, K.P. Williams, J. Chem. Soc. Perkin Trans. 2 (1981) 852.
[20] (a) P. Chen, M. Curry, T.J. Meyer, Inorg. Chem. 28 (1989) 2271; (b) P. Chen, T.J. Meyer, manuscript in preparation.
[21] J.R. Schoonover, G.F. Strouse, P. Chen, W.D. Bates, T.J. Meyer, Inorg. Chem. 32 (1993) 2618.
[22] R.E. Hester, K.P.J. Williams, J. Chem. Soc., Perkin II (1981) 852.
[23] (a) S.L. Mecklenberg, B.M. Peek, J.R. Schoonover, C.G. Wall, B.W. Erickson, T.J. Meyer, J. Am. Chem. Soc. 115 (1993) 5479; (b) S.L. Mecklenberg, D.G. McCafferty, J.R. Schoonover, B.M. Peek, B.W. Erickson, T.J. Meyer, Inorg. Chem. 33 (1994) 2974.
[24] (a) B.M. Peek, G.T. Ross, S.W. Edwards, G.J. Meyer, T.J. Meyer, B.W. Erickson, Int. J. Peptide Protein Res. 38 (1991) 114; (b) S.L. Mecklenburg, B.M. Peek, B.W. Erickson, T.J. Meyer, J. Am. Chem. Soc. 113 (1991) 854.
[25] C.A. Bignozzi, S. Roffia, C. Chiorboli, J. Davila, M.T. Indelli, F. Scandola, Inorg. Chem. 28 (1989) 4350.

[26] (a) R. Amadelli, R. Argazzi, C.A. Bignozzi, F. Scandola, J. Am. Chem. Soc. 112 (1990) 7099; (b) B. O'Regan, M. Grätzel, Nature 353 (1991) 737; (c) Sol. Energy Mater. Sol. Cells (1994) 32.
[27] C.A. Bignozzi, R. Argazzi, C.G. Garcia, F. Scandola, J.R. Schoonover, T.J. Meyer, J. Am. Chem. Soc. 114 (1992) 8727.
[28] C.A. Bignozzi, R. Argazzi, C. Chiorboli, F. Scandola, R.B. Dyer, J.R. Schoonover, T.J. Meyer, Inorg. Chem. 33 (1994) 1652.
[29] J.R. Schoonover, C.A. Bignozzi, unpublished results.
[30] P. Glyn, P.M. George, P.M. Hodges, J.J. Turner, J. Chem. Soc. Chem. Commun. (1989) 1655.
[31] J.R. Schoonover, G.F. Strouse, K.M. Omberg, R.B. Dyer, Comments Inorg. Chem. 18 (1996) 165.
[32] J.R. Schoonover, W.D. Bates, G.F. Strouse, P. Chen, R.B. Dyer, T.J. Meyer, Inorg. Chem. 35 (1995) 273.
[33] (a) J.R. Shaw, R.H. Schmehl, J. Am. Chem. Soc. 113 (1991) 389; (b) R.M. Leasure, L. Sacksteder, D. Nesselrodt, G.A. Reitz, J.N. Demas, B.A. DeGraff, Inorg. Chem. 30 (1991) 3722; (c) L. Sacksteder, A.P. Zipp, E.A. Brown, J. Streich, J.N. Demas, B.A. DeGraff, Inorg. Chem. 29 (1990) 4335; (d) A. Juris, I.B. Campagna, J.-L. Lehn, R. Ziessel, Inorg. Chem. 27 (1988) 4007; (e) S.M. Fredericks, J.C. Luong, M.S. Wrighton, J. Am. Chem. Soc. 101 (1979) 7415; (f) P.J. Giordano, M.S. Wrighton, J. Am. Chem. Soc. 101 (1979) 2889; (g) P.J. Giordano, S.M. Fredericks, M.S. Wrighton, D.L. Morse, J. Am. Chem. Soc. 100 (1978) 2257.
[34] K.C. Gordon, J.R. Schoonover, R.B. Dyer, unpublished results.
[35] W.D. Bates, Ph.D. dissertation, The University of North Carolina, Chapel Hill, 1994.
[36] R. Duesing, Ph.D. dissertation, The University of North Carolina, Chapel Hill, 1991.
[37] C.A. Bignozzi, R. Argazzi, J.R. Schoonover, K.C. Gordon, R.B. Dyer, F. Scandola, Inorg. Chem. 31 (1992) 5260.